5-1-1994

FREQUENCY OFFSET COMPENSATION AND BURST DESIGN IN FREQUENCY FLAT FADING CHANNELS

Wen-yi Kuo
Purdue University School of Electrical Engineering

Michael P. Fitz
Purdue University School of Electrical Engineering

Frequency Offset Compensation and Burst Design in Frequency Flat Fading Channels

Wen-yi Kuo
Michael P. Fitz

TR-EE 94-19
May 1994

School of Electrical Engineering
Purdue University
West Lafayette, Indiana 47907-1285

FREQUENCY OFFSET COMPENSATION AND BURST DESIGN IN FREQUENCY FLAT FADING CHANNELS*

Wen-yi Kuo and Michael P. Fitz

School of Electrical Engineering

Purdue University

West Lafayette, IN ***47907-1***285

email: wenyi@ecn.purdue.edu, mpfitz@ecn.purdue.edu

FAX: (317)-494-6440

* This work was supported by NSF under Grant NCR 91**15820.**

TABLE OF CONTENTS

Page

LIST OF TABLES

LIST OF FIGURES

Figure Page

ABSTRACT

Capability to combat channel fading and easy implementation have made the pilot symbol assisted modulation **(PSAM)** of practical interest in mobile communications. However, the operation in burst mode for multiple access purpose has still been a missing part from previous research. This work first examines the burst design problem associated with pilot symbol allocation in a frequency flat fading environment. Explicit relationship between error performance and the design parameters including pilot distribution, frequency offset, Doppler spread, and modulation scheme is explored. A new unequal spacing pilot insertion burst architecture is proposed to achieve better error performance.

Frequency offset compensation in **PSAM** is another major investigation in this work. In a mobile fading environment, conventional frequency tracking loops suffer lost-track or false lock frequently. Recent research has tried on using the consistent phase error in the correlations of pilots to estimate the frequency offset. However, the optimal frequency offset estimation in mobile fading channels is still absent from previous reports and is a major focus of this work. Frequency offset estimators with high performance and reduced complexity are studied. This work also focuses on the performance improvement of a frequency offset estimator and a Doppler spread estimator. The performance degradation investigated can be used to determine the specification of the frequency offset estimator and Doppler spread estimator used in **PSAM.** Implementing a high performance frequency offset estimator in a fading-channel receiver can significantly relieve the specification of the local oscillator and significantly improve the error performance and throughput rate.

1. INTRODUCTION

Spectrum scarcity is always a problem for wireless communication engineering and any system architecture deployed should provide bandwidth efficient communications. A common way to achieve this efficiency is invoking a large modulation alphabet (e.g., 16-QAM) and an efficient multiple access technique. For mobile and personal communications, two popular such architectures that provide the desired multiple access characteristics are time division multiple access (TDMA) and slow frequency hopped code division multiple access (SFH/CDMA). The common characteristics of these two architectures are the burst mode structure of the transmissions. The short transmission length for each burst and the demodulation over a large constellation signal set impose the barricades of achieving both near optimum error performance and high throughput efficiency. The undesired characteristics of the mobile fading channel make digital signaling an even more difficult task. This work investigates several possible improvements that can be used in the architectures for mobile digital communications.

1.1 Communication over Mobile Fading Channel

Multipath transmission is a key characteristic in mobile wireless channel. The waves traveling from the transmitter to the receiver encounter reflection due to the surrounding objects and deflection due to the media property and result in a time varying channel impulse response. The signal at the receiver input is a sum of many replicas of the transmitted signal with different delays and amplitude losses. The perceived signals add up in a random fashion depending on the various phase differences of incident waves.

The amplitude variation of the received signal is termed fading. From time to time the arriving waveforms might sum up destructively and cause the resulting amplitude to be highly attenuated. This situation is usually referred to as a deep fade. The most important feature of the deep fade is that the phase of the received signal will change rapidly and the demodulation of the phase is less immune to the noise due to the very small amplitude. Consequently, deep fades account for the dominant impairments in fading channel communication.

Two key parameters describing the mobile fading channel are the delay spread and the Doppler spread. Delay spread is due to the different lengths of the wave-traveling paths and will result in an intersymbol interference (ISI). The reciprocal of the delay spread is termed the coherence bandwidth over which the suffered fading remains approximately the same. A typical solution to prevent the delay spread detriment (i.e., ISI) is to utilize the narrowband transmission where the bandwidth of the transmitted signal is smaller than the coherence bandwidth and the signal will encounter a frequency-nonselective (or frequency-flat) fading.

Doppler spread is caused by the relative motion of the propagation path between the transmitter and the receiver. In land mobile communications, the vehicle motion is the source for this phenomenon. The Doppler spread is approximately given as (in Hz)

$$f_D = \frac{v}{\lambda} = \frac{f_c v}{C} \tag{1.1}$$

where v is the relative speed between the transmitter and the receiver, λ is the wavelength, f_C is the carrier frequency, and C is the speed of the light. The reciprocal of the Doppler spread is phrased the coherence time during which the fading process is highly correlated. A fading is considered slow if the symbol duration is much smaller than the coherence time.

The fading is caused by the superposition of plane waves from various angles. As a consequence of the central limit theory, the equivalent baseband received signal can be

viewed as a complex Gaussian random process. A fading is thus classified as Rician fading if there exists a line of sight or an equivalent dominant reflection for transmission, or else classified as Rayleigh fading if not the case. A satellite land mobile channel is typically considered a Rician fading channel but a metropolitan land-based mobile channel is usually modeled as a Rayleigh fading channel due to its complicated surroundings (e.g., buildings).

Diversity is an effective way to combat channel fading since the probability that two or more independent received signals suffer deep fade at the same instance is very low. However, the added complexity or bandwidth is the cost to pay. Besides, the optimal combining of independent received signals requires certain level of perfect synchronization. For one, the carrier frequency recovery is important in this situation.

This work considers narrowband digital communications on land mobile channels and such channels have been accurately modeled as imposing a time-varying multiplicative distortion (MD) process upon the transmitted signal. Rayleigh fading is investigated in this work since metropolitan cellular system is the chief solution to the demand for personal communications but the extension to Rician fading is straightforward. Also note, in general, Rician fading is easier to overcome than Rayleigh fading due to the existence of the dominant component in Rician fading.

The most significant problem in narrowband fading channel communications is to produce an estimate of the time-varying MD for demodulation. Techniques for estimating the MD process include Kalman filter [2, 18], block processing (e.g., Maximum Likelihood Sequence Estimation (MLSE)) [9, 11, 13], differential detection [13, 19], nonlinear processing [33], transmitted references, and combination of these. Some of the algorithms calls for only simple complexity but with a loss in performance (even an error floor in bit error probability (BEP)) while others might pay higher cost in complexity to achieve optimal performance. Among them, the one with satisfactory performance and reasonable complexity are the transmitted reference schemes.

Consequently, this work examines only the digital signaling with the transmitted references.

1.2 Synchronization by Transmitted References

Transmitted reference schemes are classified into two major groups. The one using time-multiplexing is called pilot symbol assisted modulation (PSAM) [1, 5, 26] which inserts pilot (known) symbols into the transmitted data stream. The other utilizing frequency-multiplexing is named tone calibration technique (TCT) [6, 12, 14] which transmits a pilot tone with the transmitted signal. Both of the techniques use the pilot signal in the receiver as a reference to generate the MD estimate. TCT requires extra bandwidth for the pilot tone while PSAM reduces the throughput rate as a cost to accommodate the pilot symbols. In general, both systems achieve the same performance with equivalent resource cost (power and bandwidth consumption). Nevertheless, implementation of TCT calls for the addition of a pilot tone filter while realization of PSAM necessitates the annexation of a digital pilot extractor (i.e., a clecimator). Obviously PSAM is favored in implementation due to the advantage of the digital processing techniques and will be studied in details in this work. However, the revision for TCT is forthright.

These transmitted reference techniques have been well investigated for continuous transmissions but no significant results have been reported for burst mode applications. Recent research [1, 5] has suggested the pilot symbols be spread out uniformly, i.e., inserted periodically, in a continuous transmission to improve the error performance. This work will study the shortcoming of this periodic pilot insertion structure in burst mode applications and propose a new unequal spacing frame structure for a better performance in burst mode operation.

1.3 Review of Freauency Estimation

Almost all previous work on transmitted reference techniques assumed that frequency offset between the transmitter and receiver produced negligible performance degradation. This assumption imposes in some cases a severe accuracy set specification on the radio frequency oscillators and inflates the cost. However, if a less accurate oscillator is employed and a compensation for the frequency offset is not implemented, a significant loss in performance or in throughput rate would result. A solution to this dilemma is a frequency offset estimation mechanism to relieve the stringent requirement on the oscillators.

The traditional method of frequency estimation is to employ an automatic frequency tracking loop [3, 17, 27, 29] in the receiver. The inherent closed loop structure will acquire the desired parameter slowly due to the false lock problem [34]. Besides, signals passing through the mobile fading channel experience fading distortion on the amplitude and disturbance on the phase. As mentioned above, the deep fade situation happens frequently and makes the conventional frequency tracking loop suffer a larger estimation error variance, an error floor in bit error probability (BEP), and a longer acquisition time.

Some recent efforts [4, 9, 10, 15, 21, 23] have been made on utilizing the correlations of transmitted references to estimate the frequency offset. The idea is that the sample autocorrelation functions of the pilot symbols will demonstrate a consistent phase rotation due to the frequency offset. From the phase component of the sample autocorrelation functions, the frequency offset can be obtained. However, these algorithms either are designed for non-fading AWGN channels or only use the one-step sample autocorrelation function of transmitted references for mobile fading channels. None of the previous research has studied the optimal estimation of frequency offset in mobile fading environment. Neither has investigated the benefit of utilizing multiple lag correlations of transmitted references to estimate the frequency offset over mobile fading

channels. These two missing parts are also the major focuses of this work. This work also investigates the performance effect of imperfect carrier frequency recovery and the related compensation.

1.4 Thesis Overview

This work addresses three principle issues of transmitted reference based digital communications in wireless mobile environment. First, the explicit formula of bit error probability (BEP) performance as a function of both the pilot symbols' allocation within a burst and the frequency offset uncertainty is derived. Second, the optimum allocation of the pilot symbols within the burst based on the trade-off between BEP performance and information throughput rate is investigated. Third, the optimal and reduced complexity frequency offset estimation in both continuous mode and burst mode operation is studied. A burst in this work stands for either an user slot in TDMA or a hop in SFH/CDMA.

The remainder of this document is organized as follows. Chapter 2 introduces the analytical models. Chapter 3 develops the BEP formulas for performance analysis. Chapter 4 investigates the frame design problems. Chapter 5 studies the maximum likelihood frequency offset estimator and its approximation in continuous mode operation. Chapter 6 investigates the reduced complexity frequency offset estimator based on the correlations of transmitted references. Chapter 7 contributes to the burst mode operation of frequency offset estimation and examines the performance effect of frequency offset compensation. Chapter 8 is the summary remarks and some ideas for future research.

2. ANALYTICAL MODELS

2.1 Transmitted Signal

Figure *2.1* is a block diagram of the analytical model for a PSAM based communication system. Linear modulations are considered and the transmitted signal has the form

$$s(t) = \sum_i d_i u(t - iT) \tag{2.1}$$

where $u(t)$ represents a square root unit energy Nyquist pulse shape[1] and T is the symbol duration. The complex valued d_i's are the transmitted modulation symbols and are taken from a MPSK or M-QAM alphabet (denoted as Ξ_d) where the d_i's are Gray coded and are normalized such that $E\left\{|d_i|^2\right\} = \log_2 M$. The d_i's are also assumed to be i.i.d. random variables since interleaving is common in fading channel communications. For the cases considered in detail in this work, the information bearing d_i's are characterized by

$$\begin{aligned}
d_i &= I_i^{(1)} && \text{for BPSK} \\
d_i &= I_i^{(1)} + jI_i^{(2)} && \text{for QPSK} \\
d_i &= \sqrt{\frac{2}{5}}\left\{2\left(I_i^{(1)} + jI_i^{(2)}\right) + I_i^{(1)}I_i^{(3)} + jI_i^{(2)}I_i^{(4)}\right\} && \text{for } 16-\text{QAM} \\
d_i &= \sqrt{\frac{1}{7}}\left\{4\left(I_i^{(1)} + jI_i^{(2)}\right) + 2\left(I_i^{(1)}I_i^{(3)} + jI_i^{(2)}I_i^{(4)}\right) + I_i^{(1)}I_i^{(3)}I_i^{(5)} + I^{(2)}I_i^{(4)}I_i^{(6)}\right\} && \text{for 64-QAM}
\end{aligned} \tag{2.2}$$

where $I_i^{(k)}$ is the kth information bit at time i and takes the value of ± 1.

---

[1] $R_u(nT) = \int_{-\infty}^{\infty} u(t)u^*(t - nT)dt = \delta_n$

For explanation on the gain factor in (2.2), it is assumed that the signal alphabet for 16-QAM takes the form

$$\left\{d_i = G(a_i + jb_i) \middle| a_i \text{ and } b_i = \pm 1 \text{ or } \pm 3\right\}. \tag{2.3}$$

By the symmetry of the constellation, averaging over the first quadrant leads to the balance of the energy of the d_i's, i.e.,

$$4 = E\left[\left|d_i\right|^2\right] = \frac{G^2(2+10+10+18)}{4} \tag{2.4}$$

and hence $G = \sqrt{\frac{2}{5}}$ for 16-QAM. Similarly, we can have $G = \sqrt{\frac{1}{7}}$ for 64-QAM.

Since the rotational symmetry of the signal set produces a potential phase ambiguity, PSAM is used to achieve near coherent demodulation. The known pilot symbols of PSAM are inserted in the transmitted symbols to help the demodulator derive a channel state estimate. The values of the known pilot symbols are typically randomized [26] for spectral shaping and interference suppression purposes. However, the demodulator is assumed to have the knowledge of the actual values of the transmitted pilot symbols.

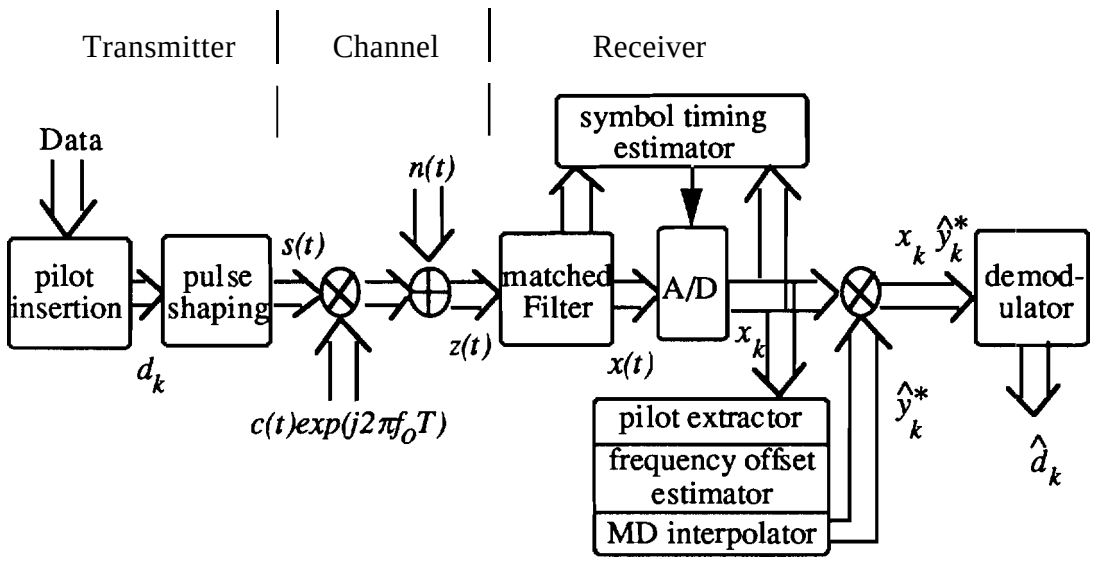

Figure 2.1. Block diagram of a pilot symbol assisted communication system.

2.2 Channel Model

The channel model for this work is the frequency nonselective, time-varying, isotropic scattering, Rayleigh fading channel with a possible frequency offset between the transmitter and receiver. With this channel, the input to the receiver is given by

$$z(t) = e^{j2\pi f_o t} c(t) s(t) + n(t) \tag{2.5}$$

where $c(t)$ is a complex Gaussian multiplicative distortion (MD), f_o is a random variable representing the unknown frequency offset with a density $p_{f_o}(f_o)$, and $n(t)$ is a complex AWGN process with one-sided spectral density N_0. The processes $n(t)$ and $c(t)$ and the random variable f_o are jointly and individually independent of each other. The isotropic Rayleigh scattering assumption implies that $c(t)$ is characterized by the Fourier transform pair [22]

$$R_c(z) = E\left\{c(t)c^*(t-\tau)\right\} = \overline{E}_b J_0\left(2\pi f_D \tau\right) \tag{2.6}$$

$$S_c(f) = \frac{\overline{E}_b}{\pi f_D}\left(1 - \frac{f^2}{f_D^2}\right)^{-\frac{1}{2}} \qquad |f| < f_D \tag{2.7}$$

where f_D represents the Doppler spread and $\overline{E}_b$ is the average received energy per bit. The asterisk (*) denotes the complex conjugate operation. Frequency spectrum of (2.7) is usually referred to as the U-shape fading spectrum.

2.3 Matched Filter Operation

The first step in the demodulation process is to pass the received signal (2.5) through a filter matched to the pulse shape $u(t)$. The sampled output of the matched filter then is

$$\begin{aligned} x_k &= x(kT) = \int_{-\infty}^{\infty} z(t)u^*(t-kT)dt \\ &= \sum_i d_i \int_{-\infty}^{\infty} c(t)e^{j2\pi f_0 t} u(t-iT)u^*(t-kT)dt + \int_{-\infty}^{\infty} n(t)u^*(t-kT)dt. \end{aligned} \tag{2.8}$$

This work assumes perfect symbol timing recovery and a first-order approximation that the pulse shape is narrow compared to $1/f_D$ so that the MD is approximately constant for a pulse duration and the ISI produced by the MD is negligible. With these assumptions, the output samples take the following form

$$\begin{aligned} x_k &= d_k c_k e^{j2\pi f_0 kT} \int_{-\infty}^{\infty} e^{j2\pi f_0 t} |u(t)|^2 dt + n_k \\ &= d_k c_k e^{jk\Omega} \xi_u(\Omega) + n_k = d_k y_k + n_k \end{aligned} \tag{2.9}$$

where c_k is a discrete time Gaussian process with $E[c_k c_{k-m}^*] = R_c(mT)$, $\Omega = 2\pi f_D T$ is the normalized radian frequency offset (radians/sample), $\xi_u(\Omega)$ is the amplitude loss caused by the frequency offset for the pulse shape $u(t)$, and n_k is a white Gaussian noise sequence with variance N_0. Note that

$$y_k = \xi_u(\Omega) c_k e^{jk\Omega} \tag{2.10}$$

denotes the discrete time total MD which includes the effect of fading and frequency offset and

$$R_y(m) = E[y_k y_{k-m}^*] = \overline{E}_{eff} J_0(2\pi f_D T m) E[e^{j\Omega m}] \tag{2.11}$$

where $\overline{E}_{eff} = \overline{E}_b \xi_u(\Omega)^2$. Notice that the fluctuation of $\xi_u(\Omega)$ due to Ω is insignificant and $\xi_u(\Omega)$ is approximated as a constant, ξ_u, independent of Ω in this work. $\gamma_{eff} = \overline{E}_{eff}/N_o$ denotes the average signal energy per bit to noise spectral density ratio.

Figure 2.2 demonstrates the hop (for SFH/CDMA) or user slot (for TDMA) structure of the PSAM burst mode communication systems considered in this work. The N pilot symbols are located at positions $p_1, p_2, \ldots, p_N$ and the data symbols are located in the remainder of the positions. The pilot symbols are used to estimate the MD and coherently demodulate the information symbols. For notation purpose, the vector of pilot symbol matched filter outputs and the vector of associated total MD's are denoted as

$$\begin{aligned} \mathbf{x}_p &= [x_{p_1}, x_{p_2}, \ldots, x_{p_N}]^T \\ \mathbf{y}_p &= [y_{p_1}, y_{p_2}, \ldots, y_{p_N}]^T. \end{aligned} \tag{2.12}$$

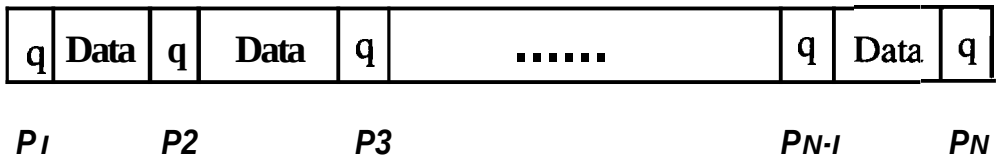

Figure 2.2. ***A*** **general burst structure of a pilot symbol assisted communication system. The q's stand for the pilot symbols and are located at the** p_i**th positions.**

3. DEMODULATION PERFORMANCE WITH PSAM

3.1 Optimal MD Interpolator

The goal of the demodulator is to retrieve the d_k's. If y_k is known, the optimum demodulator takes the form

$$\hat{d}_k = dec.\left[x_k y_k^*\right] = arg \min_{d_k \in \Xi_d} \left| d_k |y_k|^2 - x_k y_k^* \right|, \tag{3.1}$$

i.e., a decision process to find the d_k in the signal set such that $d_k|y_k|^2$ is closest to $x_k y_k^*$. A major task of the demodulator is to generate a good estimator of y_k given $\mathbf{x}_p$. Since (2.9) demonstrates a linear Gaussian model, PSAM utilizes the linear minimum mean square error (LMMSE) interpolator[2] [32] which is given as

$$\hat{y}_k = \mathbf{r}(k)\mathbf{R}_p^{-1}\mathbf{x}_p \tag{3.2}$$

where

$$\begin{aligned} \mathbf{r}(k) &= E\left[y_k \mathbf{x}_p^H\right] = E\left[y_k \mathbf{y}_p^H\right]\mathbf{\Lambda}_p^* \\ \mathbf{R}_p &= E\left[\mathbf{x}_p \mathbf{x}_p^H\right] = \mathbf{\Lambda}_p E\left[\mathbf{y}_p \mathbf{y}_p^H\right]\mathbf{\Lambda}_p^* + N_0 \mathbf{I}_N \end{aligned} \tag{3.3}$$

and $\mathbf{I}_N$ is the $N \times N$ identity matrix and $\mathbf{\Lambda}_p = diag\left(d_{p_1}, d_{p_2}, ..., d_{p_N}\right)$ is the pilot symbol data matrix. Recall that the second order moments of y_k's are given in (2.11) and are functions of the distribution of the frequency offset. The important difference between (3.2) and the optimal interpolators given in [5] is that (3.2) accounts for the random frequency offset modeled in (2.5).

---

[2] When no frequency offset is modeled and c_k is a complex Gaussian process, the linear MMSE interpolator produces the minimum BEP.

3.2 Error Probability Formula for BPSK and QPSK

Since both x_k and $\hat{y}_k$ (linear combination of pilot symbols) are complex Gaussian random variables given Ω, BEP calculations are straightforward by using the quadratic form of complex Gaussian random variables [28, 31]. Due to the rotational symmetry, the conditional BEP for BPSK of the kth data symbol in a burst is

$$BEP(k|\Omega) = P\left\{\hat{d}_k \neq d_k|\Omega\right\} = P\left\{\mathrm{Re}[x_k\hat{y}_k^*] < 0|d_k = 1,\Omega\right\}$$
$$= \frac{1}{2}\left(1 - \frac{\mathrm{Re}[\rho(1,\Omega)]}{\sqrt{1-\mathrm{Im}[\rho(1,\Omega)]^2}}\right) \tag{3.4}$$

where
$$\rho(d_k,\Omega) = \frac{E\left[x_k\hat{y}_k^*|d_k,\Omega\right]}{\sqrt{E\left[|x_k|^2|d_k,\Omega\right]E\left[|\hat{y}_k|^2|\Omega\right]}}. \tag{3.5}$$

is the correlation coefficient of x_k and $\hat{y}_k$ given d_k and R. Note that $\hat{y}_k$ is not a function of d_k. Taking expectation on Ω leads to the BEP for BPSK

$$BEP(k) = E[BEP(k|\Omega)] = \int BEP(k|\Omega)p_\Omega(\Omega)d\Omega$$
$$= \frac{1}{2}\left(1 - \int \frac{\mathrm{Re}[\rho(1,\Omega)]}{\sqrt{1-\mathrm{Im}[\rho(1,\Omega)]^2}} p_\Omega(\Omega)d\Omega\right) \tag{3.6}$$

where

$$p_\Omega(\Omega) = \frac{1}{2\pi T} p_{I_0}\left(\frac{\Omega}{2\pi T}\right) \tag{3.7}$$

is the probability distribution of R.

Numerical integration of (3.6) is possible but time consuming. An accurate and simple approximation can be developed for (3.6) by using the ideas in [8]. The key thought here is to remove the nuisance parameter Ω in (3.6) and obtain a compact form for (3.6). Note that

$$\frac{\mathrm{Re}\left[\rho(d_k,\Omega)\right]}{\sqrt{1-\mathrm{Im}\left[\rho(d_k,\Omega)\right]^2}} = \frac{\mathrm{Re}\left[\rho(d_k,\Omega)\right]}{\sqrt{\left(1-\mathrm{Im}\left[\rho(d_k,\Omega)\right]\right)\left(1+\mathrm{Im}\left[\rho(d_k,\Omega)\right]\right)}}$$
$$= \frac{\mathrm{Re}\left[\rho(d_k)\right]}{\sqrt{1-\mathrm{Im}\left[\rho(d_k)\right]^2}} \frac{1+\varepsilon_1}{\sqrt{(1+\varepsilon_2)(1+\varepsilon_3)}} \tag{3.8}$$

where

$$\rho(d_k) = E_{\Omega}\left[\rho(d_k,\Omega)\right] = \int \rho(d_k,\Omega) p_{\Omega}(\Omega) d\Omega, \tag{3.9}$$

$$\varepsilon_1 = \frac{\mathrm{Re}\left[\rho(d_k,\Omega)\right] - \mathrm{Re}\left[\rho(d_k)\right]}{\mathrm{Re}\left[\rho(d_k)\right]}, \tag{3.10}$$

$$\varepsilon_2 = \frac{\mathrm{Im}\left[\rho(d_k)\right] - \mathrm{Im}\left[\rho(d_k,\Omega)\right]}{1 - \mathrm{Im}\left[\rho(d_k)\right]}, \tag{3.11}$$

and

$$\varepsilon_3 = \frac{\mathrm{Im}\left[\rho(d_k,\Omega)\right] - \mathrm{Im}\left[\rho(d_k)\right]}{1 + \mathrm{Im}\left[\rho(d_k)\right]} \tag{3.12}$$

In all cases of interest (see later discussion), ε_i's are small enough to make the following approximation valid

$$\frac{1+\varepsilon_1}{\sqrt{(1+\varepsilon_2)(1+\varepsilon_3)}} = (1+\varepsilon_1)(1+\varepsilon_2)^{-\frac{1}{2}}(1+\varepsilon_3)^{-\frac{1}{2}} \approx 1 + \varepsilon_1 - \frac{\varepsilon_2}{2} - \frac{\varepsilon_3}{2}. \tag{3.13}$$

Since

$$E_{\Omega}\left[\varepsilon_i\right] = \int \varepsilon_i p_{\Omega}(\Omega) d\Omega = 0, \quad \forall i, \tag{3.14}$$

combining (3.6), (3.8), and *(3.13)* yields

$$BEP(k) \approx \frac{1}{2}\left(1 - \frac{\mathrm{Re}\left[\rho(1)\right]}{\sqrt{1 - \mathrm{Im}\left[\rho(1)\right]^2}}\right). \tag{3.15}$$

Define

$$Q(k) = \frac{\mathbf{r}(k)\mathbf{R}_p^{-1}\mathbf{r}(k)^H}{\overline{E}_{eff}}, \tag{3.16}$$

then

$$\begin{aligned} E\left[x_k \hat{y}_k^* \middle| d_k\right] &= E\left[\left(d_k y_k + n_k\right)\left(\mathbf{x}_p^T \mathbf{R}_p^{-1}\mathbf{r}(k)^T\right)^* \middle| d_k\right] = d_k E\left[y_k \mathbf{x}_p^H\right]\mathbf{R}_p^{-1}\mathbf{r}(k)^H \\ &= d_k \mathbf{r}(k)\mathbf{R}_p^{-1}\mathbf{r}(k)^H = d_k \overline{E}_{eff} Q(k), \end{aligned} \tag{3.17}$$

$$E\left[\left|x_k\right|^2 \middle| d_k\right] = E\left[\left(d_k y_k + n_k\right)\left(d_k y_k + n_k\right)^* \middle| d_k\right] = \left|d_k\right|^2 \overline{E}_{eff} + N_0, \tag{3.18}$$

$$E\left[\left|\hat{y}_k\right|^2\middle|d_k\right] = E\left[\left(\mathbf{r}(k)\mathbf{R}_p^{-1}\mathbf{x}_p\right)\left(\mathbf{x}_p^T\mathbf{R}_p^{-1}\mathbf{r}(k)^T\right)^*\middle|d_k\right] = \mathbf{r}(k)\mathbf{R}_p^{-1}E\left[\mathbf{x}_p\mathbf{x}_p^H\right]\mathbf{R}_p^{-1}\mathbf{r}(k)^H$$
$$= \mathbf{r}(k)\mathbf{R}_p^{-1}\mathbf{r}(k)^H = \overline{E}_{eff}Q(k), \tag{3.19}$$

and

$$\rho(d_k) = \frac{E\left[x_k\hat{y}_k^*\middle|d_k\right]}{\sqrt{E\left[\left|x_k\right|^2\middle|d_k\right]E\left[\left|\hat{y}_k\right|^2\right]}} = \frac{d_k\overline{E}_{eff}Q(k)}{\sqrt{\left(\left|d_k\right|^2\overline{E}_{eff} + N_0\right)\overline{E}_{eff}Q(k)}}. \tag{3.20}$$

Hence the BEP for BPSK can be approximated by

$$BEP(k) \approx \frac{1}{2}\left(1 - \sqrt{\frac{Q(k)}{1+\gamma_{eff}^{-1}}}\right). \tag{3.21}$$

Similar arguments can be applied to the development of BEP for QPSK. Due to the rotational symmetry, the BEP of the in-phase bit equals the BEP of the quadrature-phase bit. Hence the BEP of the kth data symbol in a burst for QPSK is

$$BEP(k) = \frac{1}{2}P\left\{\hat{I}_k^{(1)} \neq I_k^{(1)}\right\} + \frac{1}{2}P\left\{\hat{I}_k^{(2)} \neq I_k^{(2)}\right\} = P\left\{\hat{I}_k^{(1)} \neq I_k^{(1)}\right\}. \tag{3.22}$$

Using the results for quadratic forms of complex Gaussians [28, 31] gives

$$P\left\{\hat{I}_k^{(1)} \neq I_k^{(1)}\middle|\Omega\right\} = P\left\{\mathrm{Re}\left[x_k\hat{y}_k^*\right] < 0\middle|d_k = 1+j,\Omega\right\} = \frac{1}{2}\left(1 - \frac{\mathrm{Re}\left[\rho(1+j,\Omega)\right]}{\sqrt{1-\mathrm{Im}\left[\rho(1+j,\Omega)\right]^2}}\right). \tag{3.23}$$

Similar steps as (3.8)-(3.21) lead to

$$BEP(k) \approx \frac{1}{2}\left(1 - \frac{\mathrm{Re}\left[\rho(1+j)\right]}{\sqrt{1-\mathrm{Im}\left[\rho(1+j)\right]^2}}\right) = \frac{1}{2}\left(1 - \sqrt{\frac{Q(k)}{2+\gamma_{eff}^{-1}-Q(k)}}\right). \tag{3.24}$$

Note $Q(k)=1$ corresponds to the ideal coherent demodulation and the expressions for BPSK (3.21) and QPSK (3.24) with $Q(k)=1$ match the well known BEP expressions for ideal coherent demodulation [28].

Similar results were drawn in [5], however, the formulas here are more general because they accommodate a random frequency offset. Also note that no error control

coding scheme is assumed on the data sequence. The revision to include the effect of coding is straightforward [7].

To show that the approximations leading to (3.21) and (3.24) are tight for the cases of interest, a numerical comparison was performed. In this comparison, a burst with uniformly spaced pilot symbol insertion is considered. The burst uses QPSK modulation (hence (3.24) applies) and has a length of 176 symbols, 26 of which are periodically inserted pilot symbols. Denote the number of pilot symbols in each burst as N_p, the number of data symbols in each burst as N_d, and the pilot insention period as P_{ins}, hence N_p=26, N_p+N_d=176, and P_{ins}=7 for this example. The environment considered is f_DT=0.02 and f_oT ranges from 0.01 to 0.06. Figure 3.1 shows the difference between the exact BEP (by numerical integration) and the approximation (3.24) (by calculation of Q parameter) for the center data symbol in the burst. Note that the average SNR per data bit is defined as

$$\gamma_b = \frac{\bar{E}_{eff}}{N_0}\frac{N_d + N_p}{N_d} = \frac{\gamma_{eff}}{\eta} \tag{3.25}$$

where

$$\eta = \frac{N_d}{N_d + N_p} \tag{3.26}$$

is the throughput efficiency. We can observe from Figure 3.1 that as long as the pilot insertion is sufficient enough compared to the Nyquist rate of total fading (y_k), i.e., $1/P_{ins} > 2\left(f_DT + f_oT\right)$, the approximation error is negligible. Large approximation error is encountered only when the irreducible error floor occurs. Consequently for the PSAM cases of most practical interest, the approximations resulting from (3.13) are very accurate.

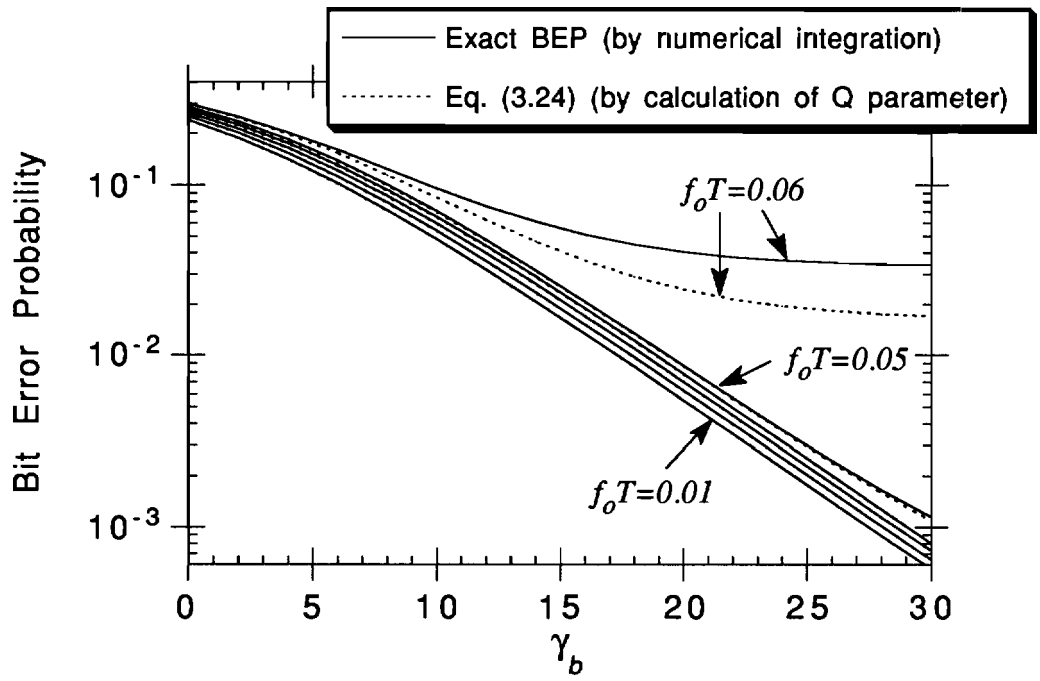

Figure 3.1 Approximation error between numeric integration and calculation of Q parameter.

3.3 Error Probability Formula for 16QAM

Again similar arguments produce expressions for the **BEP** for 16-QAM. The decision rules for 16-QAM are

$$\hat{I}_k^{(1)} = sgn\left[\mathrm{Re}\left(x_k\hat{y}_k^*\right)\right] \qquad \hat{I}_k^{(2)} = sgn\left[\mathrm{Im}\left(x_k\hat{y}_k^*\right)\right]$$
$$\hat{I}_k^{(3)} = sgn\left[\left|\mathrm{Re}\left(x_k\hat{y}_k^*\right)\right| - 2\sqrt{\frac{2}{5}}\left|\hat{y}_k\right|^2\right] \qquad \hat{I}_k^{(4)} = sgn\left[\left|\mathrm{Im}\left(x_k\hat{y}_k^*\right)\right| - 2\sqrt{\frac{2}{5}}\left|\hat{y}_k\right|^2\right] \tag{3.27}$$

where $sgn[z]=1$ when $z>0$ and $sgn[z]=-1$ when $z<0$. The rotational symmetry of the constellation implies the **BEP** of the quadrature-phase bits $(I_k^{(2)}, I_k^{(4)})$ equals the **BEP** of the in-phase bits $(I_k^{(1)}, I_k^{(3)})$ and gives the **BEP** of the *k*th data symbol in a burst as [16]

$$BEP(k) = \frac{1}{2}P\left\{\hat{I}_k^{(1)} \neq I_k^{(1)}\right\} + \frac{1}{2}P\left\{\hat{I}_k^{(3)} \neq I_k^{(3)}\right\}. \tag{3.28}$$

The individual terms can be calculated by averaging over the transmitted symbols[3] and the frequency uncertainty, **i.e.,**

$$
\begin{aligned}
P\left\{\hat{I}_k^{(i)} \neq I_k^{(i)}\right\} &= \sum_{d_k \in \Xi_d} p(d_k) P\left\{\hat{I}_k^{(i)} \neq I_k^{(i)} \middle| d_k\right\} \\
&= \frac{1}{4} \sum_{\substack{\sqrt{2.5} d_k = 1+j,\ 1+3j, \\ 3+j, or\ 3+3j}} P\left\{\hat{I}_k^{(i)} \neq I_k^{(i)} \middle| d_k\right\} \\
&= \frac{1}{4} \sum_{\substack{\sqrt{2.5} d_k = 1+j,\ 1+3j, \\ 3+j, or\ 3+3j}} \int P\left\{\hat{I}_k^{(i)} \neq I_k^{(i)} \middle| \Omega, d_k\right\} p_\Omega(\Omega) d\Omega.
\end{aligned}
\tag{3.29}
$$

Eq. (3.29) can be calculated with the quadratic forms of complex **Gaussians** by first realizing

$$
P\left\{\mathrm{Re}\left[\left(x_k - n\sqrt{\frac{2}{5}}\hat{y}_k\right)\hat{y}_k^*\right] < 0 \middle| \Omega, d_k\right\} = \frac{1}{2}\left(1 - \frac{\mathrm{Re}\left[\varphi(d_k, \Omega, n)\right]}{\sqrt{1 - \mathrm{Im}\left[\varphi(d_k, \Omega, n)\right]^2}}\right) \tag{3.30}
$$

where

$$
\varphi(d_k, \Omega, n) = \frac{E\left[\left(x_k - n\sqrt{\frac{2}{5}}\hat{y}_k\right)\hat{y}_k^* \middle| d_k, \Omega\right]}{\sqrt{E\left[\left|x_k - n\sqrt{\frac{2}{5}}\hat{y}_k\right|^2 \middle| d_k, \Omega\right] E\left[\left|\hat{y}_k\right|^2 \middle| \Omega\right]}} \tag{3.31}
$$

and n = **-2, 0,** or 2. Using the abovementioned approximation in (3.8)-(3.21) leads to

$$
\begin{aligned}
\mu(n, a_k, b_k) &= \int P\left\{\mathrm{Re}\left[\left(x_k - n\sqrt{\frac{2}{5}}\hat{y}_k\right)\hat{y}_k^*\right] < 0 \middle| \Omega, d_k\right\} p_\Omega(\Omega) d\Omega \\
&\approx \frac{1}{2}\left(1 - \frac{(a_k - n)\sqrt{Q(k)}}{\sqrt{a_k^2 + b_k^2 + 2.5\gamma_{eff}^{-1} + \left(n^2 - 2na_k - b_k^2\right)Q(k)}}\right)
\end{aligned}
\tag{3.32}
$$

where $a_k = \mathrm{Re}\left[\sqrt{2.5} d_k\right]$ and $b_k = \mathrm{Im}\left[\sqrt{2.5} d_k\right]$. Now with (3.32), we can have,

---

[3] **Actually only one quadrant of the transmitted constellation needs to be considered.**

$$P\left\{\hat{I}_k^{(1)} \neq I_k^{(1)} \middle| d_k\right\} = \int P\left\{\hat{I}_k^{(1)} \neq I_k^{(1)} \middle| \Omega, d_k\right\} p_\Omega(\Omega) d\Omega$$
$$= \int P\left\{\mathrm{Re}\left[x_k \hat{y}_k^*\right] < 0 \middle| \Omega, d_k\right\} p_\Omega(\Omega) d\Omega \qquad (3.33)$$
$$= \mu\left(0, a_k, b_k\right)$$

for the first information bit with a_k=1 or *3*,

$$P\left\{\hat{I}_k^{(3)} \neq I_k^{(3)} \middle| a_k = 1, b_k\right\} = \int P\left\{\left|\mathrm{Re}\left[x_k \hat{y}_k^*\right]\right| > 2\sqrt{\frac{2}{5}}\left|\hat{y}_k\right|^2 \middle| \Omega, a_k = 1, b_k\right\} p_\Omega(\Omega) d\Omega$$
$$= \int P\left\{\mathrm{Re}\left[\left(x_k - 2\sqrt{\frac{2}{5}}\hat{y}_k\right)\hat{y}_k^*\right] > 0 \middle| \Omega, a_k = 1, b_k\right\} p_\Omega(\Omega) d\Omega$$
$$+ \int P\left\{\mathrm{Re}\left[\left(x_k + 2\sqrt{\frac{2}{5}}\hat{y}_k\right)\hat{y}_k^*\right] < 0 \middle| \Omega, a_k = 1, b_k\right\} p_\Omega(\Omega) d\Omega \qquad (3.34)$$
$$= 1 - \mu\left(2, 1, b_k\right) + \mu\left(-2, 1, b_k\right)$$

for the third information bit with a_k=1, and similarly

$$P\left\{\hat{I}_k^{(3)} \neq I_k^{(3)} \middle| a_k = 3, b_k\right\} = \int P\left\{\left|\mathrm{Re}\left[x_k \hat{y}_k^*\right]\right| < 2\sqrt{\frac{2}{5}}\left|\hat{y}_k\right|^2 \middle| \Omega, a_k = 3, b_k\right\} p_\Omega(\Omega) d\Omega \qquad (3.35)$$
$$= \mu\left(2, 3, b_k\right) - \mu\left(-2, 3, b_k\right)$$

for the third information bit with a_k=3.

Combining ***(3.29)*** with ***(3.32)-(3.35)***gives the closed form BEP expression for 16-QAM

$$BEP(k) \approx \frac{1}{2} - \frac{1}{8}\sqrt{\frac{Q(k)}{2 + 2.5\gamma_{eff}^{-1} - Q(k)}} - \frac{3}{16}\sqrt{\frac{Q(k)}{2 + 2.5\gamma_{eff}^{-1} + 7Q(k)}}$$
$$- \frac{3}{16}\sqrt{\frac{Q(k)}{10 + 2.5\gamma_{eff}^{-1} - 9Q(k)}} - \frac{3}{8}\sqrt{\frac{Q(k)}{10 + 2.5\gamma_{eff}^{-1} - Q(k)}} + \frac{5}{16}\sqrt{\frac{Q(k)}{10 + 2.5\gamma_{eff}^{-1} + 15Q(k)}} \qquad (3.36)$$
$$- \frac{1}{16}\sqrt{\frac{Q(k)}{18 + 2.5\gamma_{eff}^{-1} - 17Q(k)}} - \frac{3}{16}\sqrt{\frac{Q(k)}{18 + 2.5\gamma_{eff}^{-1} - 9Q(k)}} + \frac{5}{16}\sqrt{\frac{Q(k)}{18 + 2.5\gamma_{eff}^{-1} + 7Q(k)}}.$$

3.4 Error Probability Formula for 64QAM

More complex BEP expression can be similarly developed for 64-QAM modulation. By the modulation symbol characterized in (2.2), the decision rules for 64-QAM are

$$\hat{I}_k^{(1)} = sgn\left[\mathrm{Re}\left(x_k \hat{y}_k^*\right)\right] \qquad \hat{I}_k^{(2)} = sgn\left[\mathrm{Im}\left(x_k \hat{y}_k^*\right)\right]$$
$$\hat{I}_k^{(3)} = sgn\left[\left|\mathrm{Re}\left(x_k \hat{y}_k^*\right)\right| - 4\sqrt{\frac{1}{7}}\left|\hat{y}_k\right|^2\right] \qquad \hat{I}_k^{(4)} = sgn\left[\left|\mathrm{Im}\left(x_k \hat{y}_k^*\right)\right| - 4\sqrt{\frac{1}{7}}\left|\hat{y}_k\right|^2\right]$$
$$\hat{I}_k^{(5)} = sgn\left[\left|\mathrm{Re}\left(x_k \hat{y}_k^*\right)\right| - 2\sqrt{\frac{1}{7}}\left|\hat{y}_k\right|^2\right] \bullet sgn\left[\left|\mathrm{Re}\left(x_k \hat{y}_k^*\right)\right| - 6\sqrt{\frac{1}{7}}\left|\hat{y}_k\right|^2\right] \tag{3.37}$$
$$\hat{I}_k^{(6)} = sgn\left[\left|\mathrm{Im}\left(x_k \hat{y}_k^*\right)\right| - 2\sqrt{\frac{1}{7}}\left|\hat{y}_k\right|^2\right] \bullet sgn\left[\left|\mathrm{Im}\left(x_k \hat{y}_k^*\right)\right| - 6\sqrt{\frac{1}{7}}\left|\hat{y}_k\right|^2\right].$$

Again, the rotational symmetry of the constellation implies the BEP of the quadrature-phase bits ($I_k^{(2)}, I_k^{(4)}, I_k^{(6)}$) behaves exactly the same way as the BEP of the in-phase bits ($I_k^{(1)}, I_k^{(3)}, I_k^{(5)}$) and this fact yields the BEP of the kth data symbol in a burst for 64-QAM as [16]

$$BEP(k) = \frac{1}{3}P\left\{\hat{I}_k^{(1)} \neq I_k^{(1)}\right\} + \frac{1}{3}P\left\{\hat{I}_k^{(3)} \neq I_k^{(3)}\right\} + \frac{1}{3}P\left\{\hat{I}_k^{(5)} \neq I_k^{(5)}\right\}. \tag{3.38}$$

Averaging over the frequency uncertainty and the first quadrant of the transmitted constellation gives the individual terms in *(3.38)*

$$P\left\{\hat{I}_k^{(i)} \neq I_k^{(i)}\right\} = \sum_{d_k} p\left(d_k\right) P\left\{\hat{I}_k^{(i)} \neq I_k^{(i)} \middle| d_k\right\}$$
$$= \frac{}{16} \sum_{\sqrt{7}d_k = a_k + jb_k} \int P\left\{\hat{I}_k^{(i)} \neq I_k^{(i)} \middle| \Omega, d_k\right\} p_\Omega(\Omega) d\Omega. \tag{3.39}$$

where $a_k = \mathrm{Re}\left[\sqrt{7}d_k\right]$ and $b_k = \mathrm{Im}\left[\sqrt{7}d_k\right]$ and both take the value of 1, 3, 5, or 7.

Similar expression as *(3.32)* for 64-QAM can be easily obtained as

$$\mu\left(n, a_k, b_k\right) = \int P\left\{\mathrm{Re}\left[\left(x_k - n\sqrt{\frac{1}{7}}\hat{y}_k\right)\hat{y}_k^*\right] < 0 \middle| \Omega, d_k\right\} p_\Omega(\Omega) d\Omega$$
$$\approx \frac{1}{2}\left(1 - \frac{\left(a_k - n\right)\sqrt{Q(k)}}{\sqrt{a_k^2 + b_k^2 + 7\gamma_{eff}^{-1} + \left(n^2 - 2na_k - b_k^2\right)Q(k)}}\right) \tag{3.40}$$

where n can be 0, ±2, ±4, or +6. Now with (3.40), we can have

$$
\begin{aligned}
P\left\{\hat{I}_k^{(1)} \neq I_k^{(1)} \middle| d_k\right\} &= \int P\left\{\hat{I}_k^{(1)} \neq I_k^{(1)} \middle| \Omega, d_k\right\} p_\Omega(\Omega) d\Omega \\
&= \int P\left\{\mathrm{Re}\left[x_k \hat{y}_k^*\right] < 0 \middle| \Omega, d_k\right\} p_\Omega(\Omega) d\Omega \\
&= \mu\left(0, a_k, b_k\right)
\end{aligned}
\tag{3.41}
$$

for the first information bit with $a_k = 1, 3, 5,$ or 7,

$$
\begin{aligned}
&P\left\{\hat{I}_k^{(3)} \neq I_k^{(3)} \middle| a_k = 1 \text{ or } 3, b_k\right\} \\
&= \int P\left\{\left|\mathrm{Re}\left[x_k \hat{y}_k^*\right]\right| > 4\sqrt{\frac{1}{7}}\left|\hat{y}_k\right|^2 \middle| \Omega, a_k = 1 \text{ or } 3, b_k\right\} p_\Omega(\Omega) d\Omega \\
&= \int P\left\{\mathrm{Re}\left[\left(x_k - 4\sqrt{\frac{1}{7}}\hat{y}_k\right)\hat{y}_k^*\right] > 0 \middle| \Omega, a_k = 1 \text{ or } 3, b_k\right\} p_\Omega(\Omega) d\Omega \\
&\quad + \int P\left\{\mathrm{Re}\left[\left(x_k + 4\sqrt{\frac{1}{7}}\hat{y}_k\right)\hat{y}_k^*\right] < 0 \middle| \Omega, a_k = 1 \text{ or } 3, b_k\right\} p_\Omega(\Omega) d\Omega \\
&= 1 - \mu\left(4, a_k, b_k\right) + \mu\left(-4, a_k, b_k\right)
\end{aligned}
\tag{3.42}
$$

for the third information bit with $a_k = 1$ or 3,

$$
\begin{aligned}
&P\left\{\hat{I}_k^{(3)} \neq I_k^{(3)} \middle| a_k = 5 \text{ or } 7, b_k\right\} \\
&= \int P\left\{\left|\mathrm{Re}\left[x_k \hat{y}_k^*\right]\right| < 4\sqrt{\frac{1}{7}}\left|\hat{y}_k\right|^2 \middle| \Omega, a_k = 5 \text{ or } 7, b_k\right\} p_\Omega(\Omega) d\Omega \\
&= \mu\left(4, a_k, b_k\right) - \mu\left(-4, a_k, b_k\right)
\end{aligned}
\tag{3.43}
$$

for the third information bit with $a_k = 5$ or 7,

$$
\begin{aligned}
&P\left\{\hat{I}_k^{(5)} \# I_k^{(5)} \middle| a_k = 1 \text{ or } 7, b_k\right\} \\
&= \int P\left\{2\sqrt{\tfrac{1}{7}}\left|\hat{y}_k\right|^2 < \left|\mathrm{Re}\left[x_k \hat{y}_k^*\right]\right| < 6\sqrt{\tfrac{1}{7}}\left|\hat{y}_k\right|^2 \middle| \Omega, a_k = 1 \text{ or } 7, b_k\right\} p_\Omega(\Omega) d\Omega \\
&= \int P\left\{2\sqrt{\tfrac{1}{7}}\left|\hat{y}_k\right|^2 < \mathrm{Re}\left[x_k \hat{y}_k^*\right] < 6\sqrt{\tfrac{1}{7}}\left|\hat{y}_k\right|^2 \middle| \Omega, a_k = 1 \text{ or } 7, b_k\right\} p_\Omega(\Omega) d\Omega \\
&\quad + \int P\left\{-6\sqrt{\tfrac{1}{7}}\left|\hat{y}_k\right|^2 < \mathrm{Re}\left[x_k \hat{y}_k^*\right] < -2\sqrt{\tfrac{1}{7}}\left|\hat{y}_k\right|^2 \middle| \Omega, a_k = 1 \text{ or } 7, b_k\right\} p_\Omega(\Omega) d\Omega \\
&= \int P\left\{\mathrm{Re}\left[\left(x_k - 6\sqrt{\tfrac{1}{7}}\hat{y}_k\right)\hat{y}_k^*\right] < 0 \middle| \Omega, a_k = 1 \text{ or } 7, b_k\right\} p_\Omega(\Omega) d\Omega \\
&\quad - \int P\left\{\mathrm{Re}\left[\left(x_k - 2\sqrt{\tfrac{1}{7}}\hat{y}_k\right)\hat{y}_k^*\right] < 0 \middle| \Omega, a_k = 1 \text{ or } 7, b_k\right\} p_\Omega(\Omega) d\Omega \\
&\quad + \int P\left\{\mathrm{Re}\left[\left(x_k + 2\sqrt{\tfrac{1}{7}}\hat{y}_k\right)\hat{y}_k^*\right] < 0 \middle| \Omega, a_k = 1 \text{ or } 7, b_k\right\} p_\Omega(\Omega) d\Omega \\
&\quad - \int P\left\{\mathrm{Re}\left[\left(x_k + 6\sqrt{\tfrac{1}{7}}\hat{y}_k\right)\hat{y}_k^*\right] < 0 \middle| \Omega, a_k = 1 \text{ or } 7, b_k\right\} p_\Omega(\Omega) d\Omega \\
&= \mu\left(6, a_k, b_k\right) - \mu\left(2, a_k, b_k\right) + \mu\left(-2, a_k, b_k\right) - \mu\left(-6, a_k, b_k\right)
\end{aligned}
\tag{3.44}
$$

for the fifth information bit with $a_k = 1$ *or* 7, *and*

$$
\begin{aligned}
&P\left\{\hat{I}_k^{(5)} \# I_k^{(5)} \middle| a_k = 3 \text{ or } 5, b_k\right\} \\
&= \int P\left\{\left|\mathrm{Re}\left[x_k \hat{y}_k^*\right]\right| > 6\sqrt{\tfrac{1}{7}}\left|\hat{y}_k\right|^2 \middle| \Omega, a_k = 3 \text{ or } 5, b_k\right\} p_\Omega(\Omega) d\Omega \\
&\quad + \int P\left\{\left|\mathrm{Re}\left[x_k \hat{y}_k^*\right]\right| < 2\sqrt{\tfrac{1}{7}}\left|\hat{y}_k\right|^2 \middle| \Omega, a_k = 3 \text{ or } 5, b_k\right\} p_\Omega(\Omega) d\Omega \\
&= 1 - \mu\left(6, a_k, b_k\right) + \mu\left(-6, a_k, b_k\right) + \mu\left(2, a_k, b_k\right) - \mu\left(-2, a_k, b_k\right)
\end{aligned}
\tag{3.45}
$$

for the fifth information bit with $a_k = 3$ *or* 5.

Combining (3.39)-(3.45) gives the closed form expression of the BEP for 64QAM

$$BEP(k)=\frac{1}{2}-\frac{1}{16}\sqrt{\frac{Q(k)}{2+7\gamma_{eff}^{-1}+7Q(k)}}-\frac{1}{48}\sqrt{\frac{Q(k)}{2+7\gamma_{eff}^{-1}-Q(k)}}+\frac{7}{96}\sqrt{\frac{Q(k)}{2+7\gamma_{eff}^{-1}+47Q(k)}}$$
$$-\frac{1}{8}\sqrt{\frac{Q(k)}{10+7\gamma_{eff}^{-1}-Q(k)}}-\frac{1}{24}\sqrt{\frac{Q(k)}{10+7\gamma_{eff}^{-1}-9Q(k)}}+\frac{5}{96}\sqrt{\frac{Q(k)}{10+7\gamma_{eff}^{-1}+15Q(k)}}$$
$$-\frac{3}{32}\sqrt{\frac{Q(k)}{10+7\gamma_{eff}^{-1}+71Q(k)}}-\frac{3}{32}\sqrt{\frac{Q(k)}{26+7\gamma_{eff}^{-1}-17Q(k)}}-\frac{1}{24}\sqrt{\frac{Q(k)}{26+7\gamma_{eff}^{-1}-25Q(k)}}$$
$$+\frac{7}{48}\sqrt{\frac{Q(k)}{26+7\gamma_{eff}^{-1}+23Q(k)}}-\frac{5}{96}\sqrt{\frac{Q(k)}{26+7\gamma_{eff}^{-1}-Q(k)}}+\frac{3}{32}\sqrt{\frac{Q(k)}{26+7\gamma_{eff}^{-1}+55Q(k)}}$$
$$-\frac{11}{96}\sqrt{\frac{Q(k)}{26+7\gamma_{eff}^{-1}+95Q(k)}}-\frac{1}{16}\sqrt{\frac{Q(k)}{18+7\gamma_{eff}^{-1}-9Q(k)}}-\frac{1}{48}\sqrt{\frac{Q(k)}{18+7\gamma_{eff}^{-1}-17Q(k)}}$$
$$+\frac{5}{96}\sqrt{\frac{Q(k)}{18+7\gamma_{eff}^{-1}+7Q(k)}}-\frac{7}{96}\sqrt{\frac{Q(k)}{18+7\gamma_{eff}^{-1}+31Q(k)}}-\frac{3}{32}\sqrt{\frac{Q(k)}{18+7\gamma_{eff}^{-1}+63Q(k)}}$$
$$-\frac{3}{32}\sqrt{\frac{Q(k)}{34+7\gamma_{eff}^{-1}-25Q(k)}}-\frac{1}{24}\sqrt{\frac{Q(k)}{34+7\gamma_{eff}^{-1}-33Q(k)}}-\frac{11}{96}\sqrt{\frac{Q(k)}{34+7\gamma_{eff}^{-1}+87Q(k)}}$$
$$-\frac{1}{8}\sqrt{\frac{Q(k)}{50+7\gamma_{eff}^{-1}-41Q(k)}}-\frac{5}{96}\sqrt{\frac{Q(k)}{50+7\gamma_{eff}^{-1}-49Q(k)}}+\frac{7}{96}\sqrt{\frac{Q(k)}{50+7\gamma_{eff}^{-1}-Q(k)}}$$
$$+\frac{13}{96}\sqrt{\frac{Q(k)}{50+7\gamma_{eff}^{-1}+119Q(k)}}-\frac{1}{32}\sqrt{\frac{Q(k)}{58+7\gamma_{eff}^{-1}-57Q(k)}}-\frac{3}{32}\sqrt{\frac{Q(k)}{58+7\gamma_{eff}^{-1}-49Q(k)}}$$
$$+\frac{5}{48}\sqrt{\frac{Q(k)}{58+7\gamma_{eff}^{-1}-33Q(k)}}-\frac{7}{48}\sqrt{\frac{Q(k)}{58+7\gamma_{eff}^{-1}-9Q(k)}}-\frac{3}{16}\sqrt{\frac{Q(k)}{58+7\gamma_{eff}^{-1}+23Q(k)}}$$
$$+\frac{11}{96}\sqrt{\frac{Q(k)}{58+7\gamma_{eff}^{-1}+63Q(k)}}+\frac{13}{96}\sqrt{\frac{Q(k)}{58+7\gamma_{eff}^{-1}+111Q(k)}}-\frac{1}{32}\sqrt{\frac{Q(k)}{74+7\gamma_{eff}^{-1}-73Q(k)}}$$
$$-\frac{1}{16}\sqrt{\frac{Q(k)}{74+7\gamma_{eff}^{-1}-65Q(k)}}+\frac{13}{96}\sqrt{\frac{Q(k)}{74+7\gamma_{eff}^{-1}+95Q(k)}}-\frac{1}{96}\sqrt{\frac{Q(k)}{98+7\gamma_{eff}^{-1}-97Q(k)}}$$
$$-\frac{1}{32}\sqrt{\frac{Q(k)}{98+7\gamma_{eff}^{-1}-89Q(k)}}+\frac{5}{96}\sqrt{\frac{Q(k)}{98+7\gamma_{eff}^{-1}-73Q(k)}}-\frac{7}{96}\sqrt{\frac{Q(k)}{98+7\gamma_{eff}^{-1}-49Q(k)}}$$
$$-\frac{3}{32}\sqrt{\frac{Q(k)}{98+7\gamma_{eff}^{-1}-17Q(k)}}+\frac{11}{96}\sqrt{\frac{Q(k)}{98+7\gamma_{eff}^{-1}+23Q(k)}}+\frac{13}{96}\sqrt{\frac{Q(k)}{98+7\gamma_{eff}^{-1}+71Q(k)}}. \quad (3.46)$$

4. FRAME STRUCTURE DESIGN

In this Chapter, the design of the frame structure, or in other words, how to locate the pilot symbols within a burst is investigated. To simplify the situation, the frequency offset is first assumed negligible in Sections 4.1-4.5. A conversion of the development to the situation with a stochastic frequency offset is attached in Section 4.6.

Traditional frame synchronization procedures place the known symbols in a large group (i.e., preambles, postambles, and/or midambles). Recent research on continuous transmission of PSAM [1, 5,261 show that a uniform distribution of pilot symbols within a transmission provides the best performance in time-varying fading. In Section 4.1, the BEP of this periodic pilot allocation structure will be examined under various fading environments. In burst mode operation, the uniform spacing is found not optimum in error performance and Section 4.2 proposes a new unequal pilot spacing structure to achieve better performance.

4.1 Overview of Uniform Spread Structure

To better understand BEP performance in burst mode operation with periodically inserted pilot symbols, a burst of varying size but with a fixed number of pilot symbols is considered. In this experiment, periodic PSAM implies that in Figure 2.2 the spacing between p_k and p_{k-1} is the same for each k (i.e., $p_k - p_{k-1} = P_{ins}$). A condition of fast fading (normalized Doppler spread $f_D T = 0.05$), no frequency offset ($f_o T = 0.0$), and γ_b = 20 dB is regarded. Figure 4.1 shows the BEP of the first 40 data symbols in a burst using periodic PSAM and BPSK with N_p=26. Figure 4.2(a) and (b) show the BEP of the center data symbol of the burst using periodic PSAM with N_p=26 and N_p=11 respectively.

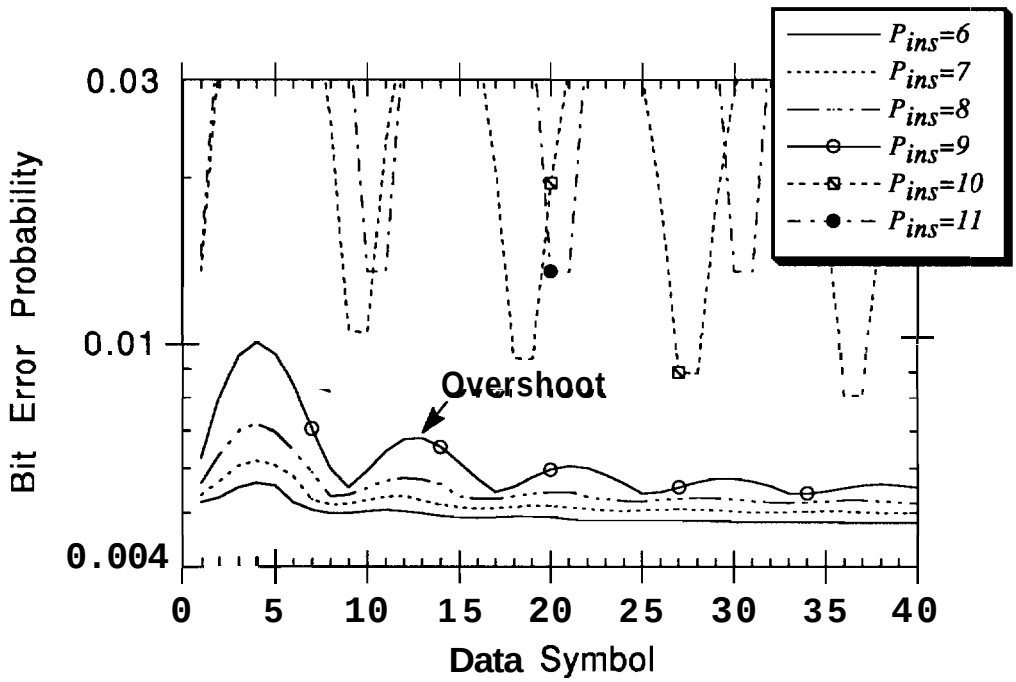

Figure 4.1. BEP curves of bursts with periodic pilot insertion and BPSK modulation. The condition evaluated is f_oT=0, f_DT=0.05, and γ_b=20dB.

Figure 4.1 and 4.2 demonstrate that the two greatest degradations of periodic PSAM in burst mode applications are the under-sampling of the fading MD and a transient increase in BEP at the burst edges. Notice in Figure 4.1 when $P_{ins} \geq (2f_DT)^{-1}$, the BEP is drastically increased as mentioned in [5]. Also observed from Figure 4.2, this threshold property is independent of the modulation scheme employed. The second degradation feature is that even if $P_{ins} < (2f_DT)^{-1}$, there is still an "overshoot" of the BEP curve in the beginning and in the end of the burst. The reason is that the MD interpolator can not provide a good MD reference due to its very asymmetrical structure in the beginning and the end of the burst. That is, the available pilot symbols are almost only on one side of the MD interpolator window and hence less smoothing of the MD process

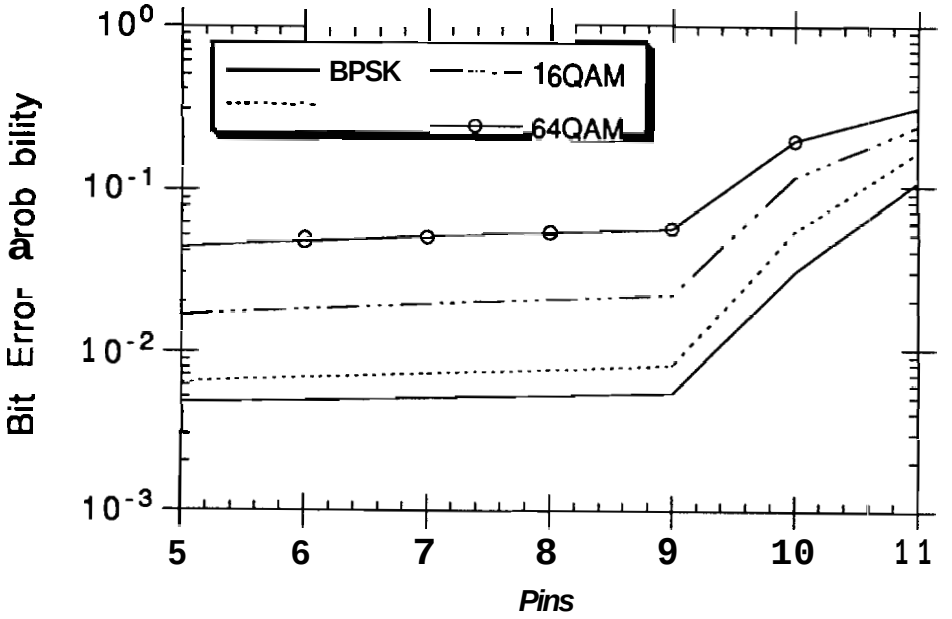

(a)

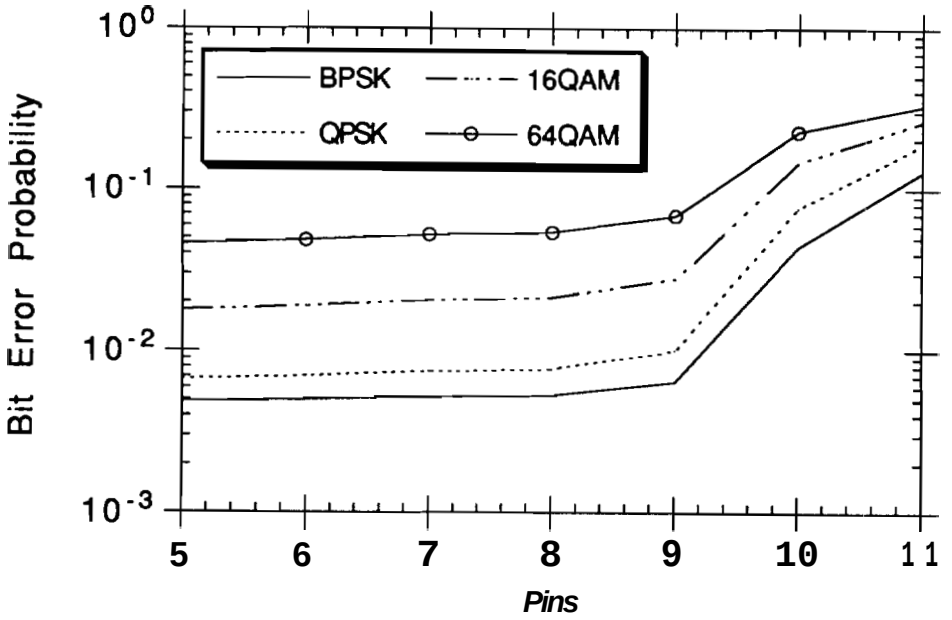

(b)

Figure 4.2 BEP of the center data symbol of the burst with periodic pilot insertion and 4 linear modulations. The condition evaluated is f_OT=0, f_DT=0.05, and γ_b=20dB. (a) Np=26. (b) Np=11.

can be achieved. Methods to reduce this overshoot phenomenon are either a decrease in the pilot insertion period or an increase in the number of pilots at the beginning and the end of a burst. However, in the middle part of the burst, the BEP behaves much like that of continuous transmission of PSAM [5] and there is no need to change the burst structure in this area. Therefore only the pilot distribution density in the two edges of a burst should be increased.

4.2 Design of Burst Structures with PSAM

Although to find an explicit formula to optimally spread the pilots in a burst is not feasible, two design rules have been discovered by experimentation to achieve better performance for burst mode communications in frequency flat fading.

The first rule is to pick a suitable pilot insertion period, P_{ins}, for the middle part of the burst by the fading aliasing free consideration, i.e., if the maximum Doppler spread encountered is f_D, P_{ins} should be an integer close to but less than $(2f_DT)^{-1}$. To eliminate large positional variations in the BEP for the middle part of the burst, P_{ins} should be one or two less than that integer. For the case considered in Figure 4.2, $(2f_DT)^{-1}=10$ and this figure demonstrates the validity of this rule. For shorter bursts (e.g., SFH/CDMA), P_{ins} should be even less to prevent a higher BEP as is shown in Figure 4.2(b).

The second rule is to assign shorter pilot insertion spacing and possibly some preamble/postamble symbols in the beginning and in the end of the burst. A general principle is found to use about a half or two thirds of P_{ins} as the first spacing and then gradually increase the size of spacing up to P_{ins}. Since the "overshoot" in the BEP curve is obvious only at the first two periods (see Figure 4.1), Figure 4.3 proposes a general frame structure for burst mode PSAM. This nonperiodic structure has shorter pilot insertion interval in the first two and the last two cycles (denoted S_1 and S_2) and L consecutive pilots in the beginning and in the end of the burst to serve as the preamble/postamble. Note that this pilot allocation is symmetric about the center of the

burst. The effect of these design parameters will be investigated in the following sections.

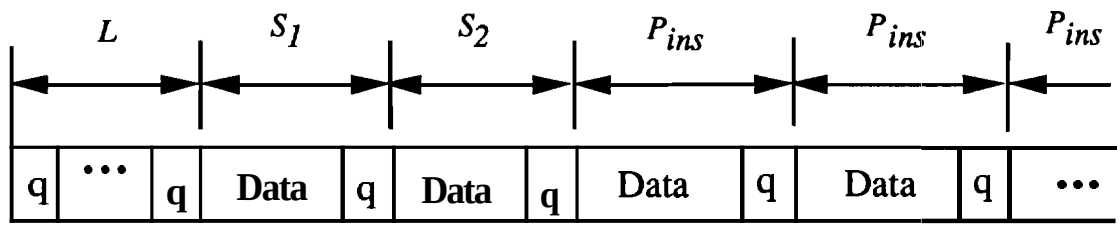

Figure 4.3 The proposed pilot allocation structure. The frame is symmetric about the center and only the beginning portion of the burst is shown. A q in the plot stands for a pilot symbol.

4.3 Design Example for Burst Mode TDMA

In this section, the design example is representative of a TDMA type architecture. For a typical burst mode TDMA application, the burst length is at the range of 150 to 200 symbols and hence the total number of pilot symbols in the burst, Np, is chosen to be 26. This number is fixed for all the examples representing TDMA applications to keep the comparison of frame structure consistent. Assuming f_DT=0.05 which implies $(2f_DT)^{-1}$ =10, then P_{ins}=7 is a good choice. Figure 4.4(a) shows the BEP for a variety of burst architectures for BPSK modulation with P_{ins}=7. Note that the BEP curves are γ_b-dependent but the relative shape is the same. A structure with good throughput efficiency and error performance for this fast fading case has L=1, S_1=5, and S_2=6. The η for this burst structure is 1441170 = 84.7% and is only slightly lower than that of periodic pilot insertion structure, 1501176 = 85.2%.

Performance in slower fading has a different characteristic from the fast fading cases presented in Figure 4.4(a). Figure 4.4(b) shows the BEP for a variety of burst architectures for f_DT = 0.01 and BPSK modulation. The key feature observed is that the pilot insertion spacing is the dominant factor of BEP in fast fading case while the

symmetry in the MD interpolator (i.e., the symmetry of the pilots around the data symbol) is the major determinant of BEP in slow fading case. This is because in fast fading cases, the pilots are tend to be very uncorrelated with the data symbol as the distance away from the data symbol exceeds several symbol durations. However, in slow fading cases, the pilot symbols which are many symbol durations away are still highly correlated with the data symbol and hence the location symmetry of the pilots around the data symbol plays a more important role.

A structure with the desired error performance (small positional variation of BEP) in slow fading has L=2 and all spacings = 7 but the associated η drops to 1381164 = 84.15%. A compromise design to fit any fading case would be L=2, S_1=5, and S_2=6 but at the cost of a lower η, 1321158 = 83.54%. For a higher throughput rate, the structure, L=1, S_1=5, and S_2=6, is a recommended choice. The tradeoff between throughput rate and BEP performance provides the flexibility of the system specifications. Since the BEP characteristics for higher order modulations (e.g., QAM) are similiar, a burst structure suitable for one linear modulation scheme is equally suitable to other linear modulation schemes.

4.4 Design Example for Burst Mode SFH/CDMA

The design for shorter burst systems such as SFH/CDMA have similar characteristics. For SFH/CDMA, typical burst lengths are of 50 to 100 symbols. With the same assumption on f_oT, a good design uses P_{ins}=7 and Np=11. The suitable burst structures either for fast fading case or for slow fading case are found to be the same as those of TDMA applications (Np=26) and are shown in Figure 4.5. Comparing Figure 4.4 with Figure 4.5 shows that Np or the burst length is not a significant factor for the design of pilot allocation. However, shorter bursts (like SFH/CDMA bursts) with the same pilot distribution structure will suffer slightly larger BEP and slightly lower throughput rate when compared to the longer bursts.

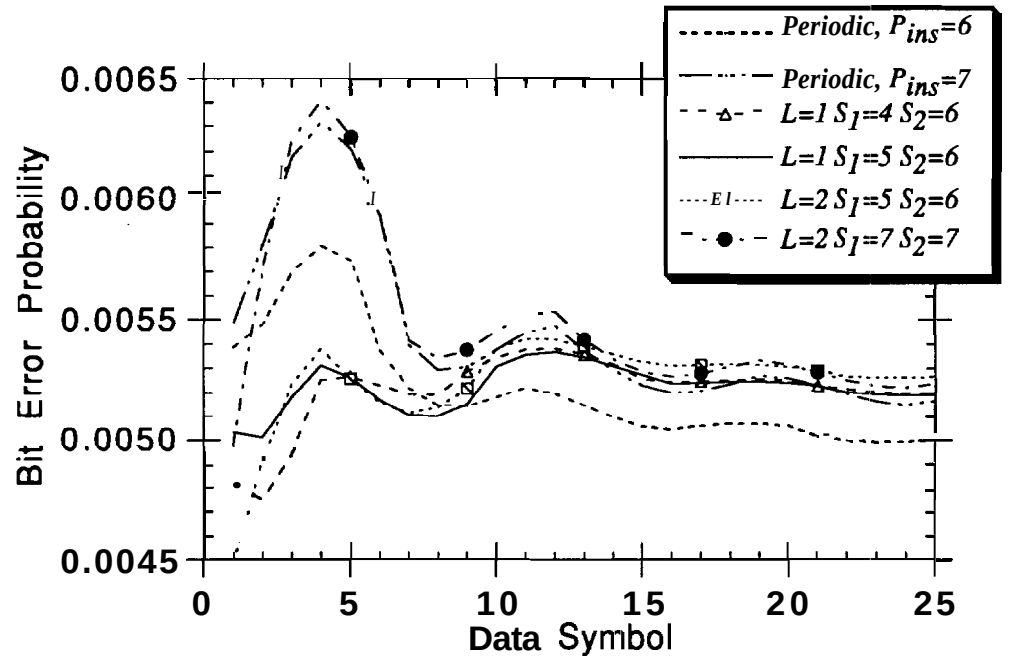

(a)

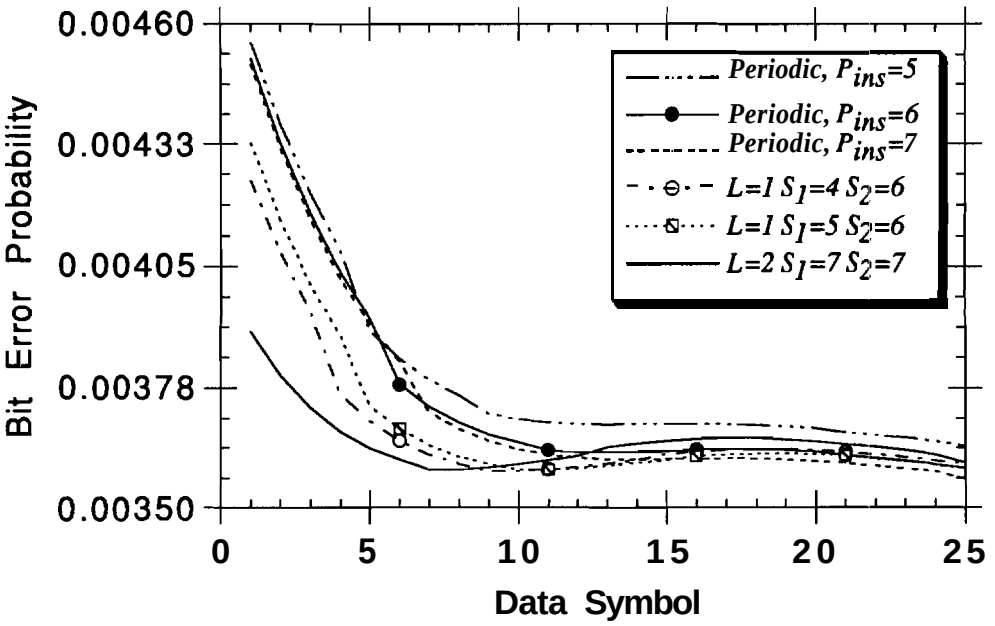

(b)

Figure 4.4 BEP curves for the first 25 data symbols of TDMA bursts with various pilot allocation structure, f_oT=0, γ_b=20dB, P_{ins}=7, Np=26, and BPSK modulation. (a) In a fast fading case, f_DT=0.05. (b) In a slow fading case, f_DT=0.01.

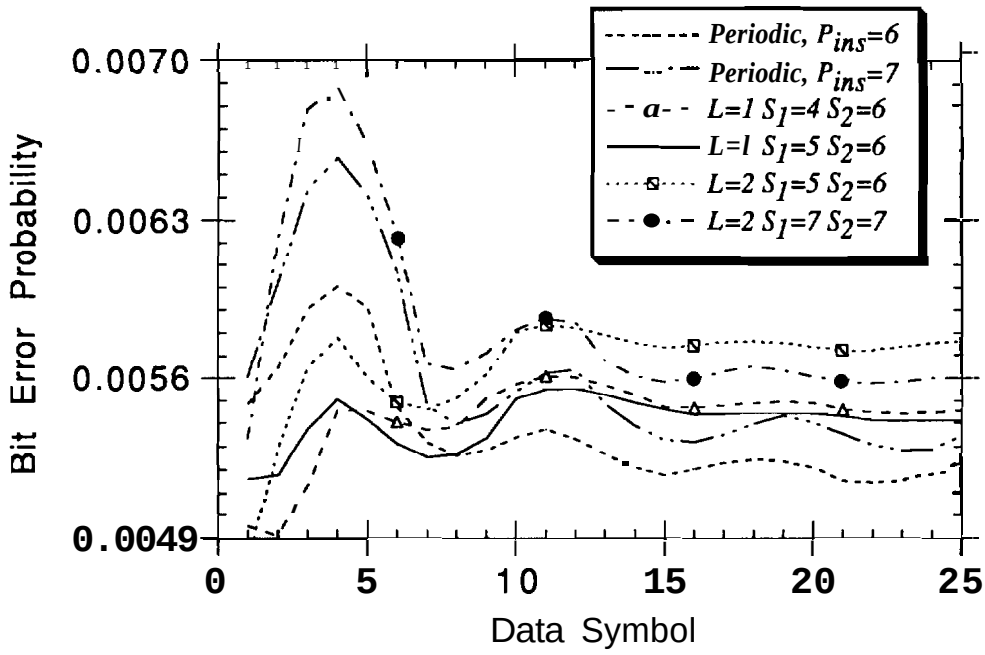

(a)

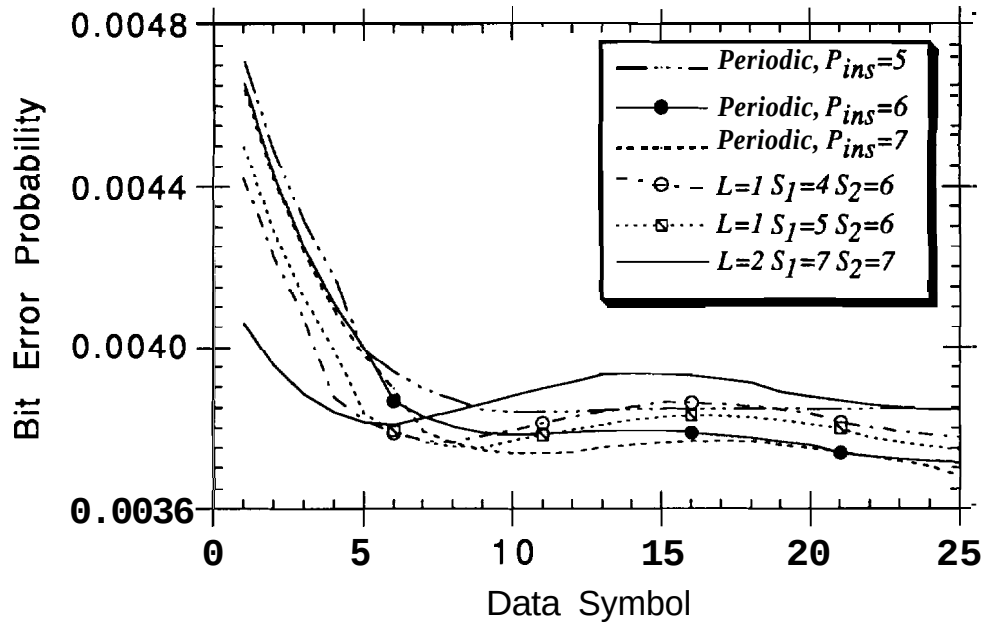

(b)

Figure 4.5 BEP curves for the first 25 data symbols of SFH/CDMA bursts with various pilot allocation structure, f_oT=0, γ_b=20dB, P_{ins}=7, Np=11, and BPSK modulation. (a) In a fast fading case, f_DT=0.05. (b) In a slow fading case, f_DT=0.01.

4.5 For Unknown Doppler Spread

Up to now, f_DT is always assumed to be known to the receiver. However, in some applications, this assumption might not be true (e.g., a cellular phone without an interface to the mobile vehicle where it mounts). This section considers the effect of a mismatch between the true Doppler spread, f_D, and the Doppler spread used to compute the interpolator coefficients, f_{AD}.

Suppose the system is targeted at the fast fading (f_DT=0.05) and no frequency offset case and the recommended frame structure (L=1, S_1=5, S_2=6, P_{ins}=7, and N_p=26) is adopted. With no knowledge about f_DT, the MD interpolator coefficients in (3.2) are calculated based on the assumed maximum Doppler spread f_{AD} and a significant difference between f_{AD} and f_D might exist. Slight modification to the BEP formula in Chapter 3 is necessary to evaluate the BEP under such a situation.

Define

$$\begin{aligned} \tilde{\mathbf{r}}(k) &= E\left[\tilde{y}_k \tilde{\mathbf{y}}_p^H\right]\mathbf{\Lambda}_p^* \\ \tilde{\mathbf{R}}_p &= \mathbf{\Lambda}_p E\left[\tilde{\mathbf{y}}_p \tilde{\mathbf{y}}_p^H\right]\mathbf{\Lambda}_p^* + N_0\mathbf{I}_N \end{aligned} \tag{4.1}$$

where

$$\begin{aligned} \tilde{\mathbf{y}}_p &= \left[\tilde{y}_{p_1}, \tilde{y}_{p_2}, \ldots, \tilde{y}_{p_N}\right]^T \\ E\left[\tilde{y}_k \tilde{y}_{k-m}^*\right] &= \overline{E}_{eff} J_0\left(2\pi f_{AD} Tm\right) E\left[e^{j\Omega m}\right]. \end{aligned} \tag{4.2}$$

The MD interpolator coefficients are optimized for $f_{AD}T$ and hence the linear MMSE interpolator of y_k in (3.2) for this case is

$$\hat{y}_k = \tilde{\mathbf{r}}(k)\tilde{\mathbf{R}}_p^{-1}\mathbf{x}_p. \tag{4.3}$$

Similar developments as those in Section 3.2 yield the BEP for BPSK as

$$\text{BEP(k)} = \frac{1}{2}\left(1 - \frac{Q_1(k)}{\sqrt{\left(1+\gamma_{eff}^{-1}\right)Q_2(k)}}\right) \tag{4.4}$$

where $$Q_1(k) = \frac{\tilde{\mathbf{r}}(k)\tilde{\mathbf{R}}_p^{-1}\mathbf{r}(k)^H}{\bar{E}_{eff}} \quad \textit{and} \quad Q_2(k) = \frac{\tilde{\mathbf{r}}(k)\tilde{\mathbf{R}}_{\hat{p}}^{-1}\mathbf{R}_p\tilde{\mathbf{R}}_p^{-1}\tilde{\mathbf{r}}(k)^H}{\bar{E}_{eff}} \tag{4.5}$$

Figure 4.6 shows the BEP curves of the cases of known Doppler spread and the cases that Doppler spread is unknown while the MD interpolator generates the MD references based on the fast fading assumption ($f_{AD}T = 0.05$). Two characteristics are noticed. The first is that the BEP increment is roughly linear proportional to the difference between f_{AD} and f_D. The second characteristics is that with the assumption that $f_{AD}T$ equals 0.05, all the BEP curves associated with unknown f_D which ranges from 0% to 5% of 1/T are almost identical and are located at where the curve of actual f_DT = 0.05 is located as shown in the top portion of Figure 4.6.

In burst mode operation, a significant performance degradation occurs; if a large mismatch between f_D and f_{AD} exists. Define SNR per bit degradation from the zero-fading case (f_DT=0) as

$$\textit{SNR/bit degradation} = 10\log_{10}\left(\frac{\textit{the } \gamma_b \textit{ needed to attain BEP} =}{\textit{the } \gamma_b \textit{ needed to attain BEP} = 10^{-3} \textit{ if } f_D = 0}\right). \tag{4.6}$$

Figure 4.7 shows the SNR/bit degradations of the center data symbol in a typical TDMA burst versus f_DT. The bottom curve in Figure 4.7 is associated with the cases that f_DT is known. The threshold jump around f_DT = 0.07 on the known f_D curve is due to the fading aliasing which occurs when $P_{ins} \geq (2f_DT)^{-1}$. The upper two curves in Figure 4.7 are associated with the cases that f_D is unknown and f_{AD} is assumed to be 3% or 5% of 1/T, respectively. When the actual f_D is smaller than f_{AD}, the γ_b needed to achieve BEP=10^{-3} is almost the same as the γ_b of the case that f_D=f_{AD}. When the actual f_D is larger than f_{AD}, it is impossible to achieve BEP = 10^{-3} (i.e., an irreducible BEP occurs) because the bandwidth of the MD interpolator is not wide enough to extract the fading information. Also note in Figure 4.7, the SNR/bit degradation for $f_D < f_{AD}$ is linear proportional to the difference between f_D and f_{AD}. Therefore the estimation of f_D is significant to fading channel synchronization with as much as 2.5 dB SNR/bit improvement.

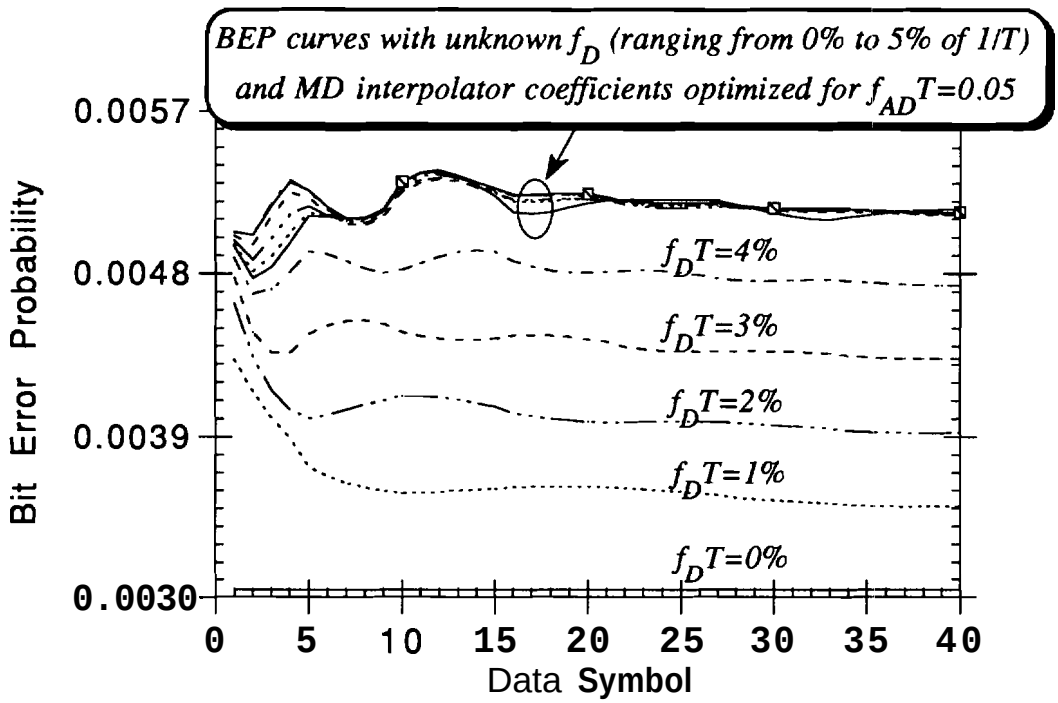

Figure 4.6 BEP curves for the first *40* data symbols of the burst with L=1, $S1$=5, $S2$=6, P_{ins}=7, and Np=26. The bottom *5* lines are associated with known f_DT. The upper most *6* curves are associated with unknown f_DT and $f_{AD}T$=0.05.

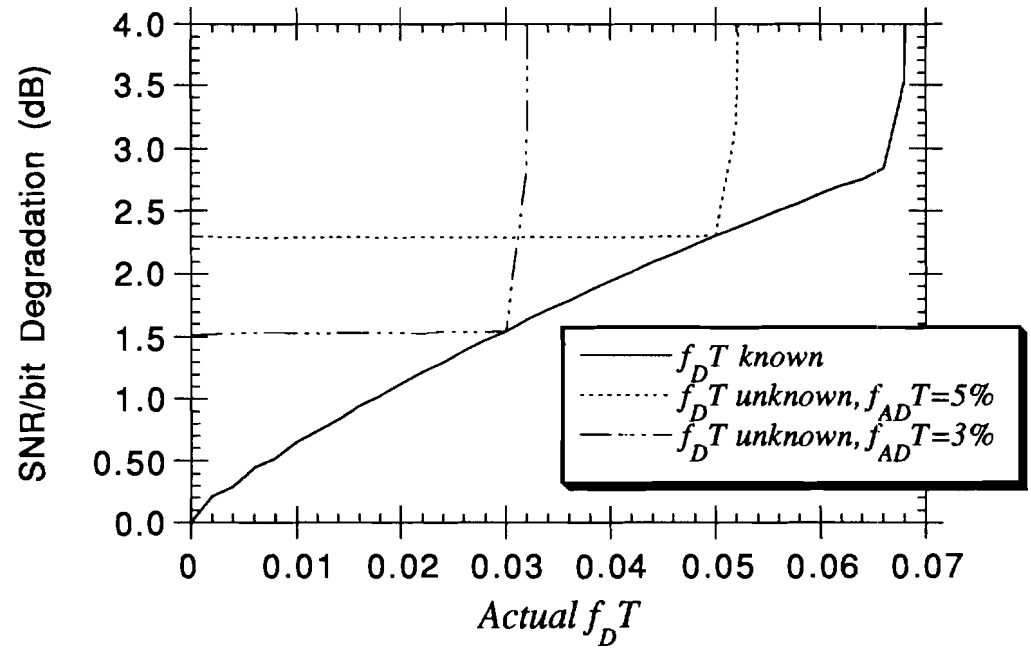

Figure 4.7 SNR degradation versus f_DT. The results are for the center data symbol of the burst with L=1, $S1$=5, $S2$=6, P_{ins}=7, Np=26, and f_oT=0.

4.6 Frame Structure with Frequency Offset

This Section examines the burst design issue with a non-trivial frequency offset. Figure 4.8 shows the frequency spectrum (normalized by $1/T$) of a baseband faded signal with a stochastic frequency offset. The normalized frequency spectrum of the faded signals is shifted away from zero by a stochastic $f_O T$. To simplify the analysis, first assume the $f_O T$ is uniformly distributed over $[-U, U]$ which accounts for the case that no frequency offset compensation is attempted as will be described in Section 7.4. From Figure 4.8, the bandwidth required by the MD interpolator without a fading aliasing error is $2(f_D T+U)$. For a frame structure not to produce an irreducible error, it must satisfy

$$P_{ins} << \frac{1}{2\left(f_D T + U\right)}. \tag{4.7}$$

This means the first burst design rule mentioned above should be changed accordingly, i.e., to pick P_{ins} to be the integer one or two less than $0.5(f_D T +U)^{-1}$. Also note that by burst design rule two, the S_1 and S_2 will be shortened correspondingly.

This fact implies that if U is non-trivial, the throughput rate will be drastically reduced. For instance, assume U=0.03 and the maximum $f_D T$ =0.05. The proper pilot allocation then is P_{ins} = 5, S_1 =3, and S_2 =4. The associated η for N_p=26 then is 94/120=78.34%, a significant loss from 85%. The reduction in frequency uncertainty is thus proved to be a necessity for a good receiver and can lead to a significant gain in throughput rate or equivalently in **BEP** performance.

For other kind of distribution of $f_O T$, the equivalent "bandwidth" of that distribution can be served as the U factor in (4.7). For the Gaussian distribution with zero mean and variance c, which will be mentioned in Section 7.4 to describe the case with frequency offset compensation, $\sqrt{\pi c/2}$ is approximately equivalent to U.

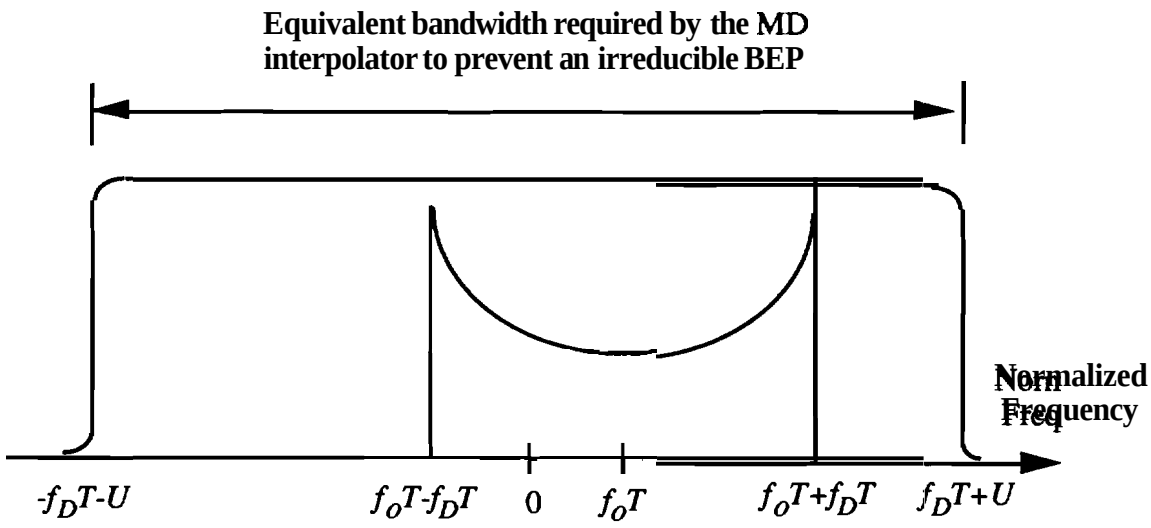

Figure 4.8 Normalized frequency spectrum of signals through a fading channel with frequency offset where f_oT is uniformly distributed over $[-U, U]$.

5. CONTINUOUS MODE MAXIMUM LIKELIHOOD FREQUENCY OFFSET ESTIMATOR

This Chapter will investigate the optimal and near-optimal frequency offset estimation. In much research [13, 19,261 done for PSAM, the carrier frequency recovery is assumed either to be perfect or to produce negligible performance degradation. However, in a real communication system, there always exists some amount of frequency offset. Many wireless communication systems have a high carrier frequency and a relatively low symbol rate. The high carrier frequency is a result of the spectrum resource assignment given by the authority (e.g., FCC) while the low data rate is due to the hardware constraint on the receiver especially for the low cost portable communicator. The combined result with the instability of the carrier frequency oscillators can create a significant baseband normalized frequency offset. For example, if the commercial specification of the local oscillator is ± 1 p.p.m. and the carrier frequency is 850 MHz, the offset frequency f_o will be within ± 850 Hz. Assume the symbol rate $(1/T)$ is 10K symbols per second. The normalized frequency offset, f_oT, then is ± 0.085, a significant number. Even if the data rate is as high as 50K symbols per second, f_oT is still ± 0.017. Section 4.5 has addressed the necessity of frequency offset compensation. The followed chapters are contributed to the study of the implementation of frequency offset compensation. The resulting performance will be examined in Chapter 7.

5.1 Continuous Mode Operation

In Chapter 5 and Chapter 6, the frequency offset estimation in continuous mode operation is considered. Continuous mode describes the situation that there are N

consecutive observations of pilot symbols available to the receiver and the frequency offset estimation is based on these N pilot symbols.

The continuous mode assumption is a general description of many applications. For instance, if the system is of periodic pilot insertion, substituting the pilot insertion period for T leads to the actual case. Another example is that at the hand-shaking stage of synchronization or at the stand-by stage, known symbols are transmitted consecutively and this situation exactly accounts for the continuous operation. In the demodulation process, some demodulation procedures utilize the decision feedback algorithm which treats the demodulated data symbol as a pilot symbol and uses the channel information it carries to estimate the time-varying MD. This example also fits the continuous mode operation assumption.

5.2 Maximum Likelihood Estimator (MLE) of Frequency Offset

In this section, the optimal frequency offset estimation in the sense of maximum likelihood will be derived. For notation purpose in continuous mode operation, define the pilot vector (the vector of pilot symbol matched filter outputs), the vector of associated MD's, and the vector of associated additive noise as

$$\begin{aligned} \mathbf{x} &= \left[x_1, x_2, \ldots, x_N\right]^T \\ \mathbf{c} &= \left[c_1, c_2, \ldots, c_N\right]^T \\ \mathbf{n} &= \left[n_1, n_2, \ldots, n_N\right]^T. \end{aligned} \tag{5.1}$$

Then the pilot vector can be written as

$$\mathbf{x} = \xi_u \mathbf{\Lambda A c} + \mathbf{n} = \mathbf{\Lambda \alpha} \tag{5.2}$$

where

$$\begin{aligned} \mathbf{A} &= diag\left(e^{j\Omega}, e^{j2\Omega}, \ldots, e^{jN\Omega}\right) \\ \mathbf{\Lambda} &= diag\left(d_1, d_2, \ldots, d_N\right) \\ \mathbf{\alpha} &= \left[\alpha_1, \alpha_2, \ldots, \alpha_N\right]^T \end{aligned} \tag{5.3}$$

and

$$\alpha_k = \frac{x_k}{d_k} = \xi_u c_k e^{jk\Omega} + \frac{n_k}{d_k} \tag{5.4}$$

is the demodulated pilot symbol (i.e., received pilot symbol with the known transmitted modulation removed). Then given the frequency offset, the mean of the pilot vector is

$$E[\mathbf{x}|\Omega] = \xi_u \mathbf{\Lambda A} E[\mathbf{c}] + E[\mathbf{n}] = 0 \tag{5.5}$$

and the autocovariance matrix is

$$\mathbf{R_x} = E\left[\mathbf{x}\mathbf{x}^H|\Omega\right] = \xi_u{}^2 \mathbf{\Lambda A} E\left[\mathbf{c}\mathbf{c}^{\mathrm{H}}\right]\mathrm{A}^{\mathrm{H}}\mathrm{A}^{\mathrm{H}} + N_o\mathbf{I} = \mathbf{A}\left(\xi_u{}^2 \mathbf{\Lambda R_c \Lambda}^H + N_o\mathbf{I}\right)\mathbf{A}^H \tag{5.6}$$

where I is an N x N identity matrix and $\mathbf{R_c} = E\left[\mathbf{c}\mathbf{c}^H\right]$. Note that

$$\det\left(\mathbf{R_x}\right) = \det\left(\xi_u{}^2 \mathbf{\Lambda R_c \Lambda}^H + N_o\mathbf{I}\right) \tag{5.7}$$

is independent of the frequency offset.

Consequently, the likelihood function for frequency estimation (i.e., the probability of the pilot vector given the frequency offset) has a Gaussian form given as

$$p(\mathbf{x}|\Omega) = \frac{1}{\pi^N \det\left(\mathbf{R_x}\right)} e^{-\mathbf{x}^H \mathbf{R_x}^{-1}\mathbf{x}} = \frac{1}{\pi^N \det\left(\mathbf{R_x}\right)} e^{\boldsymbol{\alpha}^H \mathbf{A}\mathbf{B}\mathbf{A}^H \boldsymbol{\alpha}} \tag{5.8}$$

where

$$\mathbf{B} = -\mathbf{\Lambda}^H\left(\xi_u{}^2 \mathbf{\Lambda R_c \Lambda}^H + N_o\mathbf{I}\right)^{-1}\mathbf{\Lambda} = -\left(\xi_u{}^2\mathbf{R_c} + N_o\mathbf{\Delta}\right)^{-1} \tag{5.9}$$

and

$$\mathbf{\Delta} = diag\left(\left|d_1\right|^{-2}, \left|d_2\right|^{-2}, ..., \left|d_N\right|^{-2}\right). \tag{5.10}$$

Notice that B represents the effect of Doppler spread, additive noise, and pilot modulations and is a real and symmetric matrix (i.e., $\mathbf{B}^H = \mathrm{B} = \mathrm{B}^*$). Taking log on (5.8) leads to the log-likelihood function

$$\ln\{p(\mathbf{x}|\Omega)\} = \Lambda(\mathbf{x}|\Omega) = \varsigma(\mathbf{x}) + \sum_{l=1}^{N}\sum_{k=1}^{N} e^{j(k-l)\Omega}\mathbf{B}(k,l)\alpha_k^*\alpha_l$$

$$= \varsigma(\mathbf{x}) + \sum_{n=1-N}^{N-1} e^{jn\Omega} \sum_{k=k_{mi}}^{k_{ma}} \mathbf{B}(k,k-n)\alpha_k^*\alpha_{k-n} \qquad (5.11)$$

$$= \varsigma(\mathbf{x}) + g(0) + 2\sum_{n=1}^{N-1} \mathrm{Re}\left[e^{jn\Omega} g(n)\right]$$

where

$$g(n) = \sum_{k=k_{mi}}^{k_{ma}} \mathbf{B}(k,k-n)\alpha_k^*\alpha_{k-n} \qquad (5.12)$$

is a special weighted autocorrelation function of the demodulated pilot symbols, $\varsigma(\mathbf{x})$ is some constant independent of Ω, $k_{mi} = \max\{1, n+1\}$, and $k_{ma} = \min\{N, N+n\}$. Note that $g(n)$ is conjugate symmetric about n, i.e., $g(-n)=g^*(n)$.

The maximum likelihood estimate of Ω is obtained from (5.11) as

$$\Omega_{ML} = arg \max_{\Omega} \Lambda(\mathbf{x}|\Omega). \qquad (5.13)$$

However, the global maximum of (5.11), in general, is not explicitly solvable. One way to maximize (5.11) while keeping the optimality is to employ the parallel processing techniques to the one-dimensional search. Define the candidate range as the range where the normalized frequency offset (f_OT) is possibly located. By specifying the resolution needed and searching over the candidate range, a near-optimal estimate can be obtained. Physical implementation of this method requires a bank of processors to compute (5.11) and then choose the one with the largest output as the estimate.

For instance, if we take the example mentioned above where the stability specification of the local oscillator is ± 1 p.p.m., the carrier frequency is 850 MHz, and the data rate ($1/T$) is 10K symbols per second, then f_OT is within ± 0.085 and the corresponding candidate range is [-0.085, 0.0851. If the desired resolution for f_OT estimation is 0.004, the number of the required processors or equivalently the number of the required computation paths is 43. The associated cost of this method is apparently

high especially for better resolution. Suboptimal MLE's with lower cost hence attract research attentions and will be discussed later.

5.3 Cramer-Rao Lower Bound (CRLB)

Before finding the suboptimal MLE or the approximation to MLE, the performance bound of MLE should be investigated first. Then the performance degradation from the CRLB of a suboptimal or approximated MLE can tell the quality of the estimate.

The second derivative of the log-likelihood function (5.11) is

$$\frac{d^2\Lambda(\mathbf{x}|\Omega)}{d\Omega^2} = -2\sum_{n=1}^{N-1} n^2 \,\mathrm{Re}\left[e^{jn\Omega} g(n)\right]. \tag{5.14}$$

Since

$$E[g(n)|\Omega] = \overline{E}_{eff} J_0\left(n2\pi f_D T\right) e^{-jn\Omega}\left(\sum_{k=k_{mi}}^{k_{ma}} \mathbf{B}(k,k-n)\right) \tag{5.15}$$

for any nonzero integer n, the Fisher information matrix (here, a scalar) is

$$J = -E\left[\frac{d^2\Lambda(\mathbf{x}\,|\,\Omega)}{d\Omega^2}\right] = 2\overline{E}_{eff}\sum_{n=1}^{N-1}\left\{n^2 J_0(n2\pi f_D T)\sum_{k=n+1}^{N}\mathbf{B}(k,k-n)\right\} \tag{5.16}$$

and the CRLB for the estimation of Ω is J^{-1}. In other words, if $\hat{\Omega}$ is an estimate of Ω,

$$E\left[\left(\Omega-\hat{\Omega}\right)^2\right] \geq J^{-1}. \tag{5.17}$$

5.4 Linear Approximation MLE

A linear approximation to the sine function can produce a linear frequency offset estimator in terms of the phase components of the g(n) functions. Recall a common way to maximize a function is to take the first derivative of that function and set the derivative to zero. Applying this to (5.11), the maximum likelihood equation is obtained as

$$0 = \frac{d\Lambda(\mathbf{x} \mid \Omega)}{d\Omega} = -2\,\mathrm{Im}\left(\sum_{n=1}^{N-1} n e^{jn\Omega} g(n)\right). \tag{5.18}$$

Decompose the amplitude and the phase part of the weighted autocorrelation function g(n) by defining

$$g(n) = r_n e^{j\phi_n} \qquad where \quad \phi_n = \arg\{g(n)\} \quad and \quad r_n = |g(n)|, \tag{5.19}$$

then the maximum likelihood equation (5.18) becomes

$$0 = \sum_{n=1}^{N-1} n r_n \sin(\phi_n + n\Omega). \tag{5.20}$$

In (5.12), g(n) is actually a linear combination of all n-step autocorrelation of the demodulated pilot symbols (α_k's) and Eq. (5.15) shows arg{E[g(n)|Ω]} = -nΩ. This fact suggests that, for each n, the phase of g(n) can serve as a rough estimator of Ω as long as g(n) performs close to its statistical behavior. In other words, if the number of summation terms in (5.12) is sufficient (i.e., n << N), -ϕ_n / n is a good estimate of Ω.

In non-fading or very slow fading cases, reference [15] has pointed out that for n << N, the estimator ϕ_n / n with larger lag (n) produces better estimate of Ω. This is because the behavior of the estimator ϕ_n / n can be approximated by ϕ_n / n ≈ -Ω + noise/n when n << N. However, in fast fading cases, a contrary characteristic exists. That is, the estimator ϕ_n / n with larger n produces worse estimate of Ω. This is because for larger n, the amplitude of g(n) suffers deeper fading degradation and hence the noise has more significant effect on ϕ_n / n.

Besides the above arguments, there are two more reasons that explain why only the smaller lag autocorrelation terms should be utilized. First, in the B matrix, the weighting coefficients near the diagonal are more dominant than that off the diagonal. This means the larger lag autocorrelation terms contribute less in (5.11) and are more likely to be discarded for the relief in computational burden. Second, due to the periodic nature of the estimator ϕ_n / n, any periodic image of -ϕ_n / n (i.e., - (ϕ_n +2kπ)/ n where k is

any integer) is a possible solution to the estimate of Ω. If larger lag (n) is used, more candidate solutions would result and would lead to more computational load. Hence a compromise solution that fits all situations (slow or fast fading) is to take only the first three or four ϕ_n's (i.e., $\phi_1, \phi_2, \phi_3, \phi_4$) as multiple references and combine them to form an estimate of Ω.

Figure 5.1 illustrates the performance of the estimator ϕ_n / n in both slow and fast fading cases. As a conclusion of the above discussion, the higher lag terms are removed from (5.20) for the alleviation of computational complexity and (5.20) becomes

$$0 = \sum_{n=1}^{M} n r_n \sin\left(\phi_n + n\Omega\right) \tag{5.21}$$

where M << N. By Figure 5.1, a recommended choice of M is 3 and is taken in the following development.

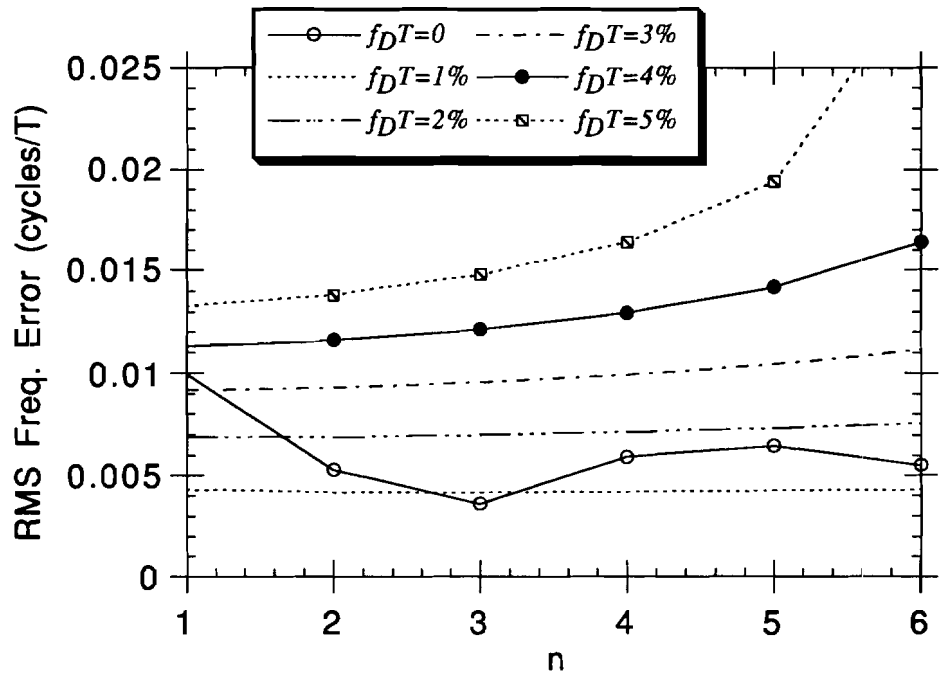

Figure 5.1 Performance of the ϕ_n / n estimators. Cases shown are of N=50, $\overline{E}_{eff}/N_0$ =20dB, 100K iterations and the f_OT before compensation can be up to 116.

Further approximation is still needed to solve (5.21). Since ϕ_n is close: to -nQ for n << N, replacing sin(x) by x in (5.21) creates a linear estimator of Ω,

$$\hat{\Omega} = -\frac{\sum_{n=1}^{M} n r_n \phi_n}{\sum_{n=1}^{M} n^2 r_n}. \qquad (5.22)$$

Figure 5.1 also reveals the fact that in very slow fading cases, $\phi_3 / 3$ produces better estimate of Ω than ϕ_1 and $\phi_2 / 2$ but in fast fading cases, ϕ_1 generates better estimate of Ω than $\phi_2 / 2$ and $\phi_3 / 3$. Hence a further simplification of (5.22), which always includes the best ϕ_n / n estimator in any fading case, is

$$\hat{\Omega} = -\frac{r_1\phi_1 + 3r_3\phi_3}{r_1 + 9r_3} \qquad (5.23)$$

Notice that all image solutions of Ω (i.e., $-(\phi_n + 2k\pi)/n$ where k is an integer such that $-(\phi_n/2\pi n + k/n)$ is in the candidate range) should be considered in (5.22) and (5.23). If the length of the candidate range is smaller than 1/3, there is only one solution. This situation is what we hope for and only requires the specification of the local oscillator be $\pm 15\%$ of $(f_c T)^{-1}$ where f_c is the carrier frequency. If f_c=850MHz and symbol rate (1/T)=10K, the stability specification requirement for the local oscillator is only ± 1.76 p.p.m. However, in general, multiple estimates of Ω generated by (5.22) or (5.23) are possible. The quickest way to decide which one is the optimal estimate of Ω is to evaluate (5.11) at each candidate solution and choose the one with the largest outcome.

5.5 Smart Start Newton Search (SSNS) MLE

Refinement on the results produced by the linear estimator can further improve the performance. Although (5.22) or (5.23) is a quick and good estimator of Ω, the performance is not satisfied by applications requiring tight precision. To irnprove the performance, some refinement algorithm can be invoked with the multiple outputs of

(5.22) or (5.23) serving as the smart starting points. In this section the well known Newton's method is the refinement algorithm considered.

The basic recursive formula of the Newton's method is

$$\hat{\Omega}_{k+1} = \hat{\Omega}_k - \frac{\frac{d}{d\Omega}\Lambda(\mathbf{x}_p|\Omega)\Big|_{\Omega=\hat{\Omega}_k}}{\frac{d^2}{d\Omega^2}\Lambda(\mathbf{x}_p|\Omega)\Big|_{\Omega=\hat{\Omega}_k}} \tag{5.24}$$

where the first and second derivatives can be found in (5.18) and (5.14) respectively. Some modification of the Newton's method is required since (5.11) is not pure quadratic. The first constraint is that the change step of Newton's method can not be larger than certain amount. This is to prevent jumping out of the local near-quadratic area. The second constraint is that the second derivative, $\frac{d^2}{d\Omega^2}\Lambda(\mathbf{x}_p|\Omega)$, can not be non-negative. In case of these occurrences, the change step is set to be a small step change in the direction of positive first derivative. After the converging iterations of (5.24), the value of (5.11) is evaluated at each multiple output points and choose the point with largest outcome of (5.11) as the estimate of Ω.

5.6 Smart Start Local Uniform Search (SSLUS) MLE

Since (5.11) is a superposition of many harmonic sinusoidals, Newton's method tends to stop at some local maximal points instead of the desired global maximal point. Another way to refine the estimates of (5.22) or (5.23), termed smart start local uniform search, is to evaluate the value of (5.11) at the neighborhood of the multiple output points of (5.22) or (5.23) and then search the point with largest value of (5.11) as the estimate of Ω. However, the local uniform search requires a parallel bank of computation paths and hence increases the computational complexity. The number of required computation paths is equal to the local search range divided by the resolution needed and times the number of multiple starting points. For example, assume the candidate range of $f_O T$ is

[-0.2, 0.2], the local search range is ±0.01, and the resolution requirement is 0.003. Then there are two possible output points of (5.22) or (5.23) and the number of the computation paths needed for local uniform search is 0.02/0.003*2=14.

6. REDUCED COMPLEXITY FREQUENCY OFFSET ESTIMATOR

Since optimal or near-optimal frequency offset estimation requires heavy computation, growing interest has been shown on the reduced complexity frequency offset estimation which uses the phases of the estimated correlations of the pilots to estimate the frequency offset. From (5.4), the autocorrelation function of the demodulated pilot symbols is

$$R_\alpha(n) = E\left[\alpha_k \alpha_{k-n}^* | \Omega\right] = \overline{E}_{eff} J_0(n2\pi f_D T) e^{jn\Omega} \tag{6.1}$$

where the phase component equals $n\Omega$ for any nonzero integer n. This fact suggests that the phase term of the estimated autocorrelation of the demodulated pilots can be used to estimate the Ω. Recently, much attention [4, 9, 10, 21] has been put on utilizing $R_\alpha(1)$ to estimate the Ω. Although the complexity of using $R_\alpha(1)$ is quite simple, the performance is not satisfied. References [15, 23] combined multiple higher lag terms (i.e., $R_\alpha(n)$ for n $\geq$ 1) to estimate Ω and lead to more satisfactory outcomes with very little increase in complexity. However, these two papers studied only the case of non-fading AWGN channels. For fading channels, the advantage of taking higher lag terms to produce better estimate of Ω has not been investigated yet and is the major focus of this Chapter.

6.1 Correlation Estimator

A correlation estimator of the demodulated pilot symbols takes the form, $\hat{R}_\alpha(n) = \sum_{k=n+1}^{N} h_k \alpha_k \alpha_{k-n}^*$, where the h_k's are the weighting coefficients and N is the number of the available demodulated pilot symbols. If the h_k is equal to B(k,k-n) for each k, $\hat{R}_\alpha^*(n)$ is equal to g(n). Although the special weighting coefficients of g(n)

performs better than the uniform weighting coefficients (i.e., h_k=the same constant, $\forall$ k), the implementation of the unequal weighting coefficients costs a significant complexity increase especially in recursive estimation application. That is, when the number of available pilots increases, say from N to $N+1$, the equal weighting case calls for only the computation of the innovation terms but the unequal weighting case as of g(n) demands all terms to be re-computed. This is because the optimal weighting coefficients in B changes with N and the transformation from $\mathbf{B}(N)$ to $\mathbf{B}(N+1)$ requires heavy computation.

In the following, the equal weighting coefficients are chosen for $\hat{R}_\alpha(n)$ but the transformation of related developments to $g(n)$ is straightforward. Now define the n-step autocorrelation estimator of the demodulated pilot symbols as

$$\hat{R}_\alpha(n|N) = \frac{1}{N-|n|}\sum_{k=k_{mi}}^{k_{ma}(N)} \alpha_k \alpha_{k-n}^* \tag{6.2}$$

for any integer n where N is the number of the available pilot symbols, $k_{mi} = \max(1, 1+n)$ and $k_{ma}(N) = \min(N, N+n)$. The recursive formula for this estimator can be obtained as

$$\hat{R}_\alpha(n|N+1) = \frac{N-|n|}{N+1-|n|}\hat{R}_\alpha(n|N) + \frac{\alpha_{k_{ma}(N+1)}\alpha^*_{k_{ma}(N+1)-n}}{N+1-|n|} \tag{6.3}$$

Notice that the updating process only requires the computation of the innovation term (the second term in the RHS of (6.3)). For relief in notation, $\hat{R}_\alpha(n)$ is used to present $\hat{R}_\alpha(n|N)$ and k is used to stand for $k_{ma}(N)$ throughout this work. Also note that

$$E\left[\hat{R}_\alpha(n)|\Omega\right] = R_\alpha(n) \quad \text{and} \quad \arg\left\{E\left[\hat{R}_\alpha(n)|\Omega\right]\right\} = n\Omega, \tag{6.4}$$

which means $\hat{R}_\alpha(n)$ is an unbiased estimate of $R_\alpha(n)$ and the phase of $\hat{R}_\alpha(n)$ can be served as a rough estimator of $n\Omega$ if n << N and N is sufficiently large.

6.2 Frequency Offset Estimator by Correlation Estimator

This section will develop a frequency offset estimator based on the phases of the estimated correlations. Define

$$\theta_n = \frac{\arg\left\{\hat{R}_\alpha(n)\right\}}{n}, \quad \boldsymbol{\theta} = \left[\theta_1, \theta_2, ..., \theta_M\right]^T, \text{ and } \quad \mathbf{1} = [1,1,...,1]^T \tag{6.5}$$

where $\boldsymbol{\theta}$ and $\mathbf{1}$ are both vectors of length M. By reference [25], θ_n can be approximated as Gaussian distributed with mean Ω if n << N and N is sufficiently large.

Suppose $\theta_1, \theta_2, ..., \theta_M$ are available and M << N. The estimate of Ω now is to find the best combination of $\theta_1, \theta_2, ..., \theta_M$. From simulations, the joint probability distribution function of $\theta_1, \theta_2, ..., \theta_M$ is found that it can be approximated by a jointly Gaussian distribution. Under such an approximation, the best combination of $8_1, \theta_2, ..., \theta_M$ to estimate Ω is a linear interpolation with coefficients from inverse of the associated covariance matrix.

By the jointly Gaussian approximation of 0, we have

$$\ln\left\{p(\boldsymbol{\theta}|\Omega)\right\} = \varepsilon' - (\boldsymbol{\theta} - \Omega\mathbf{1})^{\mathrm{T}} \mathbf{C}_{\boldsymbol{\theta}}^{-1} (0 - \mathrm{Q1}) \tag{6.6}$$

where ε' is some constant independent of 8 and C_θ is the covariance matrix of θ, i.e.,

$$\mathbf{C}_{\boldsymbol{\theta}} = E\left[(\boldsymbol{\theta} - \Omega\mathbf{1})(\boldsymbol{\theta} - \Omega\mathbf{1})^T | \Omega\right]. \tag{6.7}$$

To maximize $\ln\left\{p(\boldsymbol{\theta}|\Omega)\right\}$ is to set the first derivative of $\ln\left\{p(\boldsymbol{\theta}|\Omega)\right\}$ with respect to Ω equal to zero, i.e.,

$$0 = \frac{d}{d\Omega} \ln\left\{p(\boldsymbol{\theta}|\Omega)\right\} = \sum_{n=1}^{M}\sum_{m=1}^{M} \mathbf{C}_{\boldsymbol{\theta}}^{-1}(\mathrm{n},m)\left(\theta_n + \theta_m - 2\Omega\right). \tag{6.8}$$

Then the estimator of Ω is obtained as

$$\hat{\Omega} = \frac{\sum_{n=1}^{M}\sum_{m=1}^{M} \mathbf{C}_{\boldsymbol{\theta}}^{-1}(n,m)\left(\theta_n + \theta_m\right)}{2\sum_{n=1}^{M}\sum_{m=1}^{M} \mathbf{C}_{\boldsymbol{\theta}}^{-1}(n,m)}. \tag{6.9}$$

Actually even if $\boldsymbol{\theta}$ is not jointly Gaussian, (6.9) is still the optimal interpolator within the linear class of estimators of Ω based on θ.

6.3 Covariance Estimator

In ***(6.9)***, the only unsolved parts is C_θ^{-1}. This section is devoted to solving this matrix. Define

$$\beta_n = \frac{\hat{R}_\alpha(n)}{R_\alpha(n)} - 1 \quad \text{and hence} \quad \hat{R}_\alpha(n) = R_\alpha(n)\left(1+\beta_n\right). \tag{6.10}$$

β_n represents the normalized error between the true correlation function and the estimated correlation function of the demodulated pilot symbols. By the approximation that θ is jointly Gaussian, we have

$$\begin{aligned} E\left[\frac{\hat{R}_\alpha(n)\hat{R}_\alpha(m)}{\hat{R}_\alpha^*(n)\hat{R}_\alpha^*(m)}\right] &= E\left[e^{j2(n\theta_n+m\theta_m)}\right] = e^{j2(n+m)\Omega} \bullet e^{-0.5\,\mathrm{var}\left[2(n\theta_n+m\theta_m)\right]} \\ &= \frac{R_\alpha(n)R_\alpha(m)}{R_\alpha^*(n)R_\alpha^*(m)} E\left[\frac{(1+\beta_n)(1+\beta_m)}{(1+\beta_n^*)(1+\beta_m^*)}\right] = e^{j2(n+m)\Omega} \bullet E\left[\frac{(1+\beta_n)(1+\beta_m)}{(1+\beta_n^*)(1+\beta_m^*)}\right] \end{aligned} \tag{6.11}$$

for any nonzero integers n, m. Eliminating the common terms leads to

$$E\left[\frac{(1+\beta_n)(1+\beta_m)}{(1+\beta_n^*)(1+\beta_m^*)}\right] = e^{-0.5\,\mathrm{var}\left[2(n\theta_n+m\theta_m)\right]} \approx 1 - 2\,\mathrm{var}\left[n\theta_n + m\theta_m\right]. \tag{6.12}$$

Similarly, we can have

$$E\left[\frac{(1+\beta_n)(1+\beta_m^*)}{(1+\beta_n^*)(1+\beta_m)}\right] = e^{-0.5\,\mathrm{var}\left[2(n\theta_n-m\theta_m)\right]} \approx 1 - 2\,\mathrm{var}\left[n\theta_n - m\theta_m\right]. \tag{6.13}$$

Combining ***(6.12)*** and ***(6.13)*** yields

$$E\left[(\theta_n-\Omega)(\theta_m-\Omega)\right] \approx \frac{1}{8nm}\left\{E\left[\frac{(1+\beta_n)(1+\beta_m^*)}{(1+\beta_n^*)(1+\beta_m)}\right] - E\left[\frac{(1+\beta_n)(1+\beta_m)}{(1+\beta_n^*)(1+\beta_m^*)}\right]\right\}. \tag{6.14}$$

By series expansion, we have

$$E\left[\frac{(1+\beta_n)(1+\beta_m^*)}{(1+\beta_n^*)(1+\beta_m)}\right] = E\left[(1+\beta_n)(1+\beta_m^*)\left(\sum_{k=0}^{\infty}\left(-\beta_n^*\right)^k\right)\left(\sum_{l=0}^{\infty}\left(-\beta_m\right)^l\right)\right]$$

$$\begin{aligned}
&= E\Big[1+\beta_n+\beta_m^*-\beta_n^*-\beta_m+\beta_n\beta_m^*-\beta_n\beta_n^*-\beta_n\beta_m-\beta_n^*\beta_m^*-\beta_m\beta_m^*+\beta_m\beta_n^* \\
&\quad +\left(\beta_n^*\right)^2+\left(\beta_m\right)^2-\beta_n\beta_m^*\beta_n^*-\beta_n\beta_m\beta_m^*+\beta_n\beta_n^*\beta_m+\beta_m\beta_m^*\beta_n^*+\beta_n\left(\beta_n^*\right)^2 \\
&\quad +\beta_m^*\left(\beta_n^*\right)^2-\beta_m\left(\beta_n^*\right)^2+\beta_n\left(\beta_m\right)^2+\beta_m^*\left(\beta_m\right)^2-\beta_n^*\left(\beta_m\right)^2-\left(\beta_n^*\right)^3-\left(\beta_m\right)^3 \\
&\quad +\textit{higher order terms}\Big].
\end{aligned} \tag{6.15}$$

Intuitively from (6.10), $|\beta_n|$ is a number smaller than *1* and close to zero and $E[\beta_n] = 0$. Therefore the contributions of higher order terms can be neglected. To solve *(6.15)* now only requires to solve the second and the third moments of β_n.

The general formula for the second order moment is

$$\begin{aligned}
E\left[\beta_n\beta_m\right] &= \frac{E\left[\hat{R}_\alpha(n)\hat{R}_\alpha(m)\right]}{R_\alpha(n)R_\alpha(m)} - 1 = \frac{\sum_{k=k_{mi}}^{k_{ma}}\sum_{l=l_{mi}}^{l_{ma}} E\left[\alpha_k\alpha_{k-n}^*\alpha_l\alpha_{l-m}^*\right]}{(N-|n|)(N-|m|)R_\alpha(n)R_\alpha(m)} - 1 \\
&= \frac{\sum_{k=k_{mi}}^{k_{ma}}\sum_{l=l_{mi}}^{l_{ma}}\left\{E\left[\alpha_k\alpha_{k-n}^*\right]E\left[\alpha_l\alpha_{l-m}^*\right]+E\left[\alpha_k\alpha_{l-m}^*\right]E\left[\alpha_l\alpha_{k-n}^*\right]\right\}}{(N-|n|)(N-|m|)R_\alpha(n)R_\alpha(m)} - 1 \\
&\quad - \frac{\sum_{k=k_{mi}}^{k_{ma}}\sum_{l=l_{mi}}^{l_{ma}}\Gamma(k,l-m)\Gamma(l,k-n)}{(N-|n|)(N-|m|)\Gamma(n,0)\Gamma(m,0)}
\end{aligned} \tag{6.16}$$

where

$$\Gamma(k,l) = J_0\left((k-l)2\pi f_D T\right) + \frac{N_0}{\bar{E}_{eff}\left|d_k\right|^2}\delta(k-l), \tag{6.17}$$

$k_{mi} = \max(1, 1+n)$, $k_{ma} = \min(N, N+n)$, $l_{mi} = \max(1, 1+m)$, $l_{ma} = \min(N, N+m)$, and $\delta()$ is the kronecker delta function.

Similarly, the general formula for the third order moment is

$$E[\beta_n\beta_m\beta_s] = E\left[\left(\frac{\hat{R}_\alpha(n)}{R_\alpha(n)}-1\right)\left(\frac{\hat{R}_\alpha(m)}{R_\alpha(m)}-1\right)\left(\frac{\hat{R}_\alpha(s)}{R_\alpha(s)}-1\right)\right]$$

$$= \frac{E[\hat{R}_\alpha(n)\hat{R}_\alpha(m)\hat{R}_\alpha(s)]}{R_\alpha(n)R_\alpha(m)R_\alpha(s)} - \left(\frac{E[\hat{R}_\alpha(n)\hat{R}_\alpha(m)]}{R_\alpha(n)R_\alpha(m)}-1\right) - \left(\frac{E[\hat{R}_\alpha(m)\hat{R}_\alpha(s)]}{R_\alpha(m)R_\alpha(s)}-1\right) - \left(\frac{E[\hat{R}_\alpha(n)\hat{R}_\alpha(s)]}{R_\alpha(n)R_\alpha(s)}-1\right) - 1$$

$$- \frac{\sum_{k=k_{mi}}^{k_{ma}}\sum_{l=l_{mi}}^{l_{ma}}\sum_{u=u_{mi}}^{u_{ma}} E[\alpha_k\alpha_{k-n}^*\alpha_l\alpha_{l-m}^*\alpha_u\alpha_{u-s}^*]}{(N-|n|)(N-|m|)(N-|s|)R_\alpha(n)R_\alpha(m)R_\alpha(s)} - E[\beta_n\beta_m] - E[\beta_m\beta_s] - E[\beta_n\beta_s] - 1$$

$$- \frac{\sum_{k=k_{mi}}^{k_{ma}}\sum_{l=l_{mi}}^{l_{ma}}\sum_{u=u_{mi}}^{u_{ma}} \Gamma(l,k-n)\Gamma(u,l-m)\Gamma(k,u-s) + \Gamma(u,k-n)\Gamma(k,l-m)\Gamma(l,u-s)}{(N-|n|)(N-|m|)(N-|s|)\Gamma(n,0)\Gamma(m,0)\Gamma(s,0)} -$$

(6.18)

where $u_{mi}=\max(1,1+s)$, and $u_{ma}=\min(N,N+s)$. The calculation of the sixth order moments of α_n can be found in reference [24].

Note that all the second and third order moments of β_n are independent of R. Also notice that from *(6.2)* and *(6.10)*,

$$\hat{R}_\alpha^*(n) = \hat{R}_\alpha(-n) \quad \text{and} \quad \beta_{-n} = \beta_n^*. \tag{6.19}$$

Hence we can substitute the terms with negative index for the conjugated terms in *(6.15)* and *(6.14)* and explicitly calculate *(6.15)* and *(6.14)* based on *(6.16)* and *(6.18)*. From simulations, it is found that in (6.14), the value counted up to the second moments is slightly larger than the simulated value but the value counted up to the third moments is slightly smaller than the simulated value. To get a better estimate is to average over these two values. After grouping terms and taking the average, *(6.14)* becomes

$$E[(\theta_n-\Omega)(\theta_m-\Omega)] \approx \frac{1}{2nm}\left(E[\beta_n\beta_{-m}] - E[\beta_n\beta_m]\right) + \frac{1}{8nm}\left(E[\beta_m\beta_n\beta_n] - E[\beta_{-m}\beta_n\beta_n] + E[\beta_n\beta_m\beta_m] - E[\beta_{-n}\beta_m\beta_m]\right). \tag{6.20}$$

With (6.16)-(6.20), $\mathbf{C}_{\boldsymbol{\theta}}^{-1}$ and hence *(6.9)* can be explicitly obtained.

6.4 Simulation Result and Implementation Suggestion

Figure 6.1-6.3 show the performance of the frequency offset estimators mentioned so far in fast fading, moderate fading, and zero-fading cases respectively. Zero-fading means f_D=0 (i.e., the vehicle stands still at that moment) but the receiver is still suffering the MD due to multipath reflection of transmitted waves. Simulations of the zero-fading case still requires generating the random incident angles of arriving waves for each iteration of realization. Hence the zero-fading situation is different from the non-fading AWGN model where the c_k in (2.9) is assumed to be the same constant ($\sqrt{\bar{E}_b}$) for each simulation iteration. A larger estimation error of Ω in zero-fading case is thus expected compared to the non-fading AWGN case.

For generating the random arrival angles, reference [20] has the details. The root mean square (RMS) frequency error is obtained from simulations of 100K iterations where $\bar{E}_{eff}/N_0$=20dB. The performance by ϕ_n alone is only slightly better than that by θ_n alone and is not shown in the plots. SSLUS-1 stands for the method proposed in Section 5.6 where the local search range = ± 0.01 and search resolution = 0.002. Alternatively SSLUS-2 stands for the wider local search range (=± 0.02) but with coarser search grid (0.003). SSNS represents the Newton search method in Section 5.5.

These curves demonstrate two features. First, a near-optimal frequency offset estimate can be obtained by SSLUS. For a fixed number of total search paths, the wider local search range is suggested in fast fading cases whereas in very slow fading cases, the finer search resolution is recommended. Second, the method of (6.9) performs well in both slow and fast fading cases. Actually in the zero-fading case, the weighting coefficients of (5.22), (5.23), or (6.9) are nearly identical to the optimal coefficients shown in reference [15].

The choice of estimator depends on the detection algorithm used and performance requirement. If a recursive algorithm is employed, (6.9) is recommended because the uniform weighting in (6.2) saves a lot of computation or equivalently storage load

compared to the renewal procedure of coefficients in ***(5.12)***. However, if detection is by block processing, the burden of **SSLUS** becomes more affordable and then **SSLUS** is a favored choice. Also note that employing ***(6.9)*** requires N large enough to acquire the desired statistical behavior. If only a small number of pilot symbols is available or an extreme tight performance is required, **SSLUS** is the unique solution.

Moreover, note that f_D is quasi-static, i.e., f_D is almost a constant inside a burst since the speed of the vehicle won't change so fast but in the long run, f_D is time-varying from burst to burst. For easy implementation, the coefficients of ***(6.9)*** or ***(5.12)*** can be pre-calculated and stored in a data bank based on a grid of f_D. Then for each burst, the receiver can pick the set of coefficients of which the associated f_D is closest to the actual f_D to conduct the demodulation process.

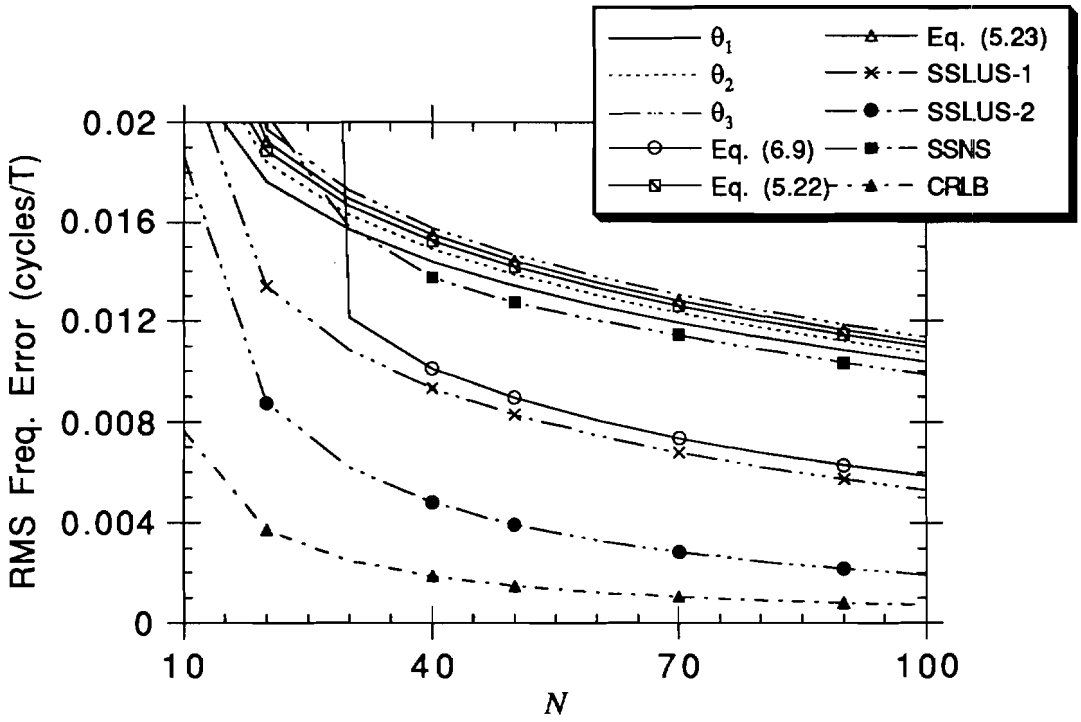

Figure ***6.1*** Performance of various estimators of Ω in fast fading case (f_DT=0.05).

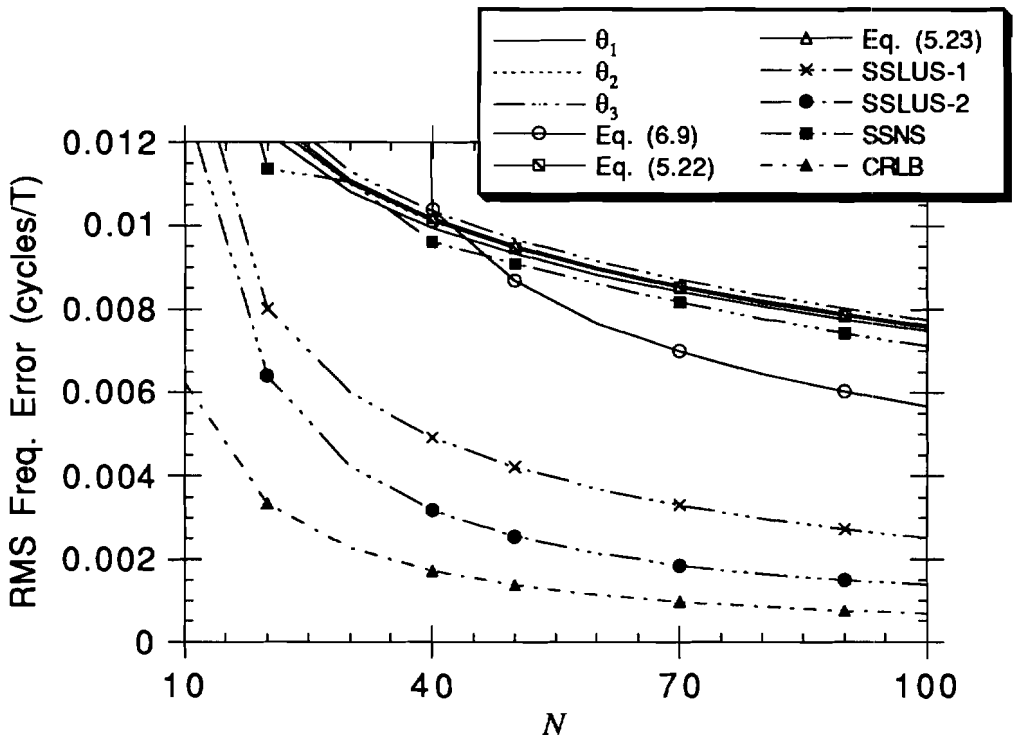

Figure *6.2* Performance of various estimators of Ω in moderate fading case (f_DT=0.03).

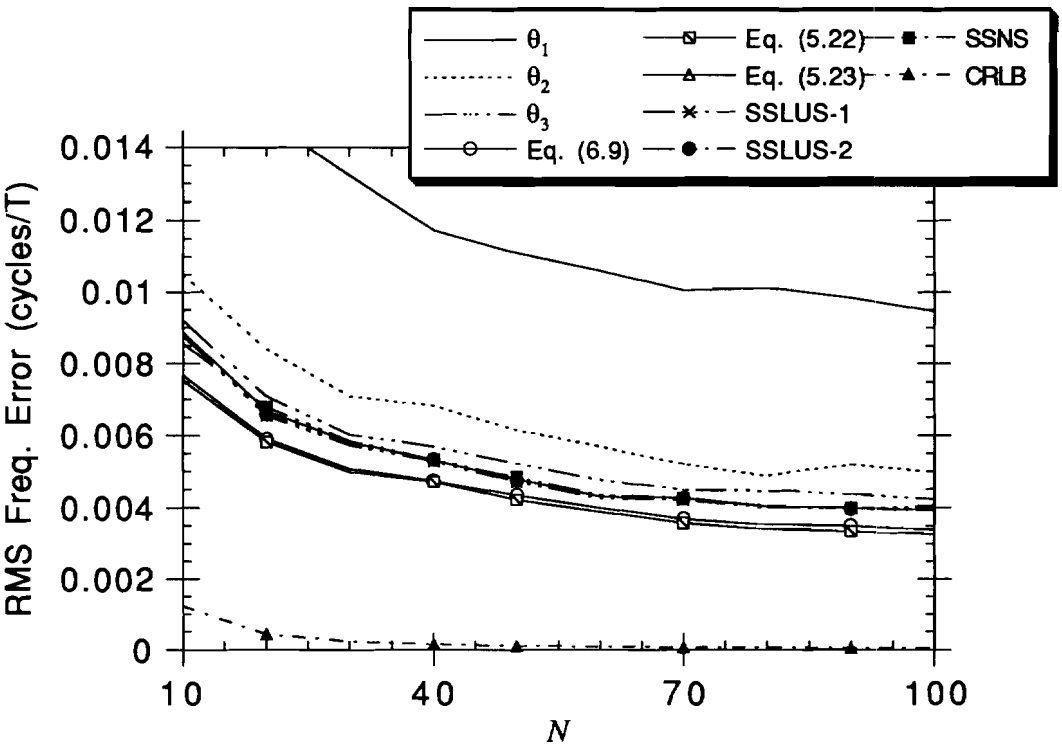

Figure *6.3* Performance of various estimators of Ω in zero-fading case (f_DT=0.0).

7. BURST MODE FREQUENCY OFFSET COMPENSATION

Since TDMA and SFH/CDMA are two popular multiple access schemes in wireless mobile communications, frequency offset estimation in burst mode operation potentially calls for practical interest and is investigated in this Chapter. The burst mode operation is to estimate the frequency offset based on the N scattered pilot symbols in a burst as shown in Figure 2.2.

7.1 Revised MLE for Burst Mode Operation

First examine the MLE in the burst mode situation where the pilot vector and the associated MD vector are as

$$\begin{aligned} \mathbf{x}_p &= \left[x_{p_1}, x_{p_2}, \ldots, x_{p_N} \right]^T \\ \mathbf{c}_p &= \left[c_{p_1}, c_{p_2}, \ldots, c_{p_N} \right]^T . \end{aligned} \tag{7.1}$$

The log-likelihood function (5.11) in this situation becomes

$$\Lambda\left(\mathbf{x}_p|\Omega\right) = \varsigma'\left(\mathbf{x}_p\right) + \sum_{l=1}^{N}\sum_{k=1}^{N} e^{j(p_k - p_l)\Omega} \mathbf{B}_p(k,l)\alpha^*_{p_k}\alpha_{p_l} \tag{7.2}$$

where

$$\mathbf{B}_p = -\left(\xi_u^2 E\left[\mathbf{c}_p \mathbf{c}_p^H\right] + N_o \Delta_p\right)^{-1}, \tag{7.3}$$

$$\alpha_{p_k} = \frac{x_{p_k}}{d_{p_k}} = \xi_u c_{p_k} e^{jp_k\Omega} + \frac{n_{p_k}}{d_{p_k}}, \tag{7.4}$$

$$\Delta_p = diag\left[\left| d_{p_1} \right|^{-2}, \left| d_{p_2} \right|^{-2}, \ldots, \left| d_{p_N} \right|^{-2} \right], \tag{7.5}$$

and $\varsigma'(\mathbf{x}_p)$ is a constant independent of R.

Then the maximum likelihood frequency offset estimator for burst mode operation is

$$\Omega_{ML} = arg \max_{\Omega} \Lambda\left(\mathbf{x}_p|\Omega\right) \tag{7.6}$$

In general, the n-step correlation function in (5.12), $g(n)$, can not be defined here because the time differences in each diagonal of $\mathbf{B}_p$ are not the same. As a result, methods of (5.22) and (5.23) can not be applied. However, a near-optimal solution still can be obtained by parallel processing which calculates (7.2) over the candidate range and choose the R with the largest value of (7.2), though the associated cost is quite high.

Revised from (5.16), the Fisher information matrix for the burst mode is

$$J_p = \overline{E}_{eff} \sum_{l=1}^{N} \sum_{k=1}^{N} \left(p_k - p_l\right)^2 \mathbf{B}_p(k,l) J_0\left(2\pi f_D T(p_k - p_l)\right) \tag{7.7}$$

and the CRLB for frequency offset estimation given $\mathbf{x}_p$ is J_p^{-1}.

7.2 For Burst Mode TDMA

This section investigates the approximation of the MLE of R for the TDMA applications. The basic idea is to use the correlation of the pilot symbols to obtain rough estimates of Ω and then refine the results by the methods introduced in Sections 5.5 and 5.6. Figure 4.3 has proposed a burst structure with unequal pilot insertion spacing to get a better BEP performance. In the middle part of the burst, the pilot symbols are inserted periodically with period P_{ins}. Hence the method used in (5.23) can be applied to the middle part of a burst. Here the recommended structure (L=1, $S1$=5, $S2$=6, P_{ins}=7, and N=26) is first considered.

Before apply a similar method as (5.23) to get the rough estimates; of R, we should learn what periodic components are good for implementation. Since P_{ins}=7 and L=1, only the pilot correlations of 7k (k=1, 2, 3, etc.) steps can be obtained. Figure 7.1 shows the performance of these periodical components where

$$\psi_n = -\frac{\arg\left\{g_p(n)\right\}}{n}, \quad \upsilon_n = \left|g_p(n)\right|, \quad and \quad g_p(n) = \sum_{l=1}^{N} \sum_{\substack{k=1 \\ p_k - p_l = n}}^{N} \mathbf{B}_p(k,l) \alpha_{p_k}^{*} \alpha_{p_l}. \tag{7.8}$$

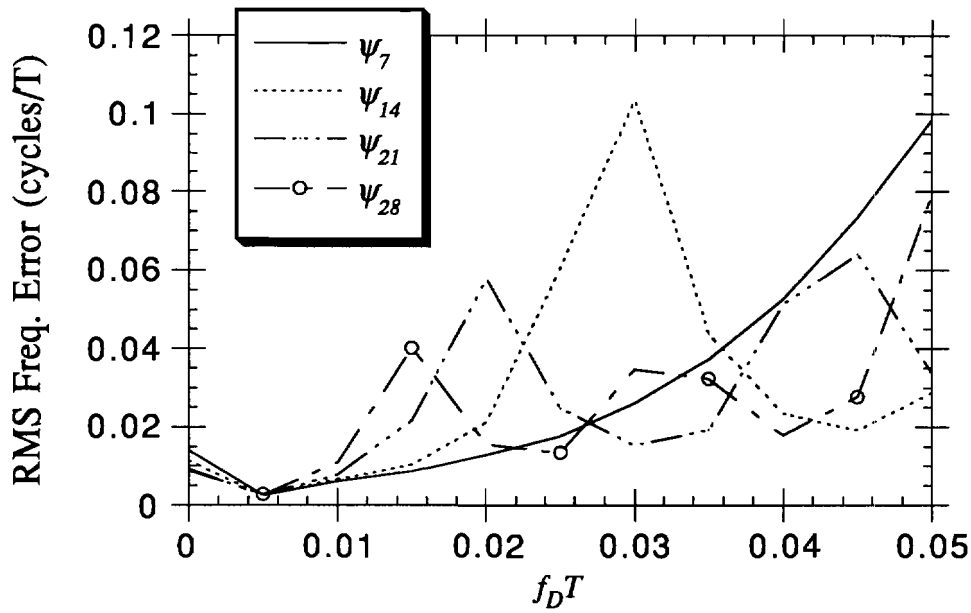

Figure 7.1 Performance of ψ_n. The case shown is for the burst with L=1, S_1=5, S_2=6, P_{ins}=7, and N=26, $\bar{E}_{eff}/N_0 = 20\text{dB}$, and 100K iterations.

Note that there are multiple image solutions of ψ_n and the one with the largest value of (7.2) is selected as the rough estimate of Ω according to the rule of maximum likelihood. However, the image solution with the largest value of (7.2) sometimes is not the image solution closest to the true frequency offset. Figure 7.2 shows a realization of the log-likelihood function as a function of $f_O T$ and the contribution of some of its components. The peak near $f_O T$=0.1 of the curve $A(\mathbf{x}_p|\Omega)$ is the desired solution. However another peak close to $f_O T$=0.1-1/7=-0.043 is an alias solution but with a fairly large value of $A(\mathbf{x}_p|\Omega)$. The situation that the estimator chooses the alias solution instead of the desired solution, termed alias frequency capture, might happen due to 1) the transient noise problem especially in a deep fade condition and 2) the inadequate number of pilot symbols such that the statistic in (7.2) does not behave like its statistical conduct. The large estimation error shown in Figure 7.1 mostly comes from the alias frequency capture effect. If all the image solutions of ψ_n are considered as the multiple starting

points of certain refinement algorithm, the alias frequency capture effect can be mostly eliminated.

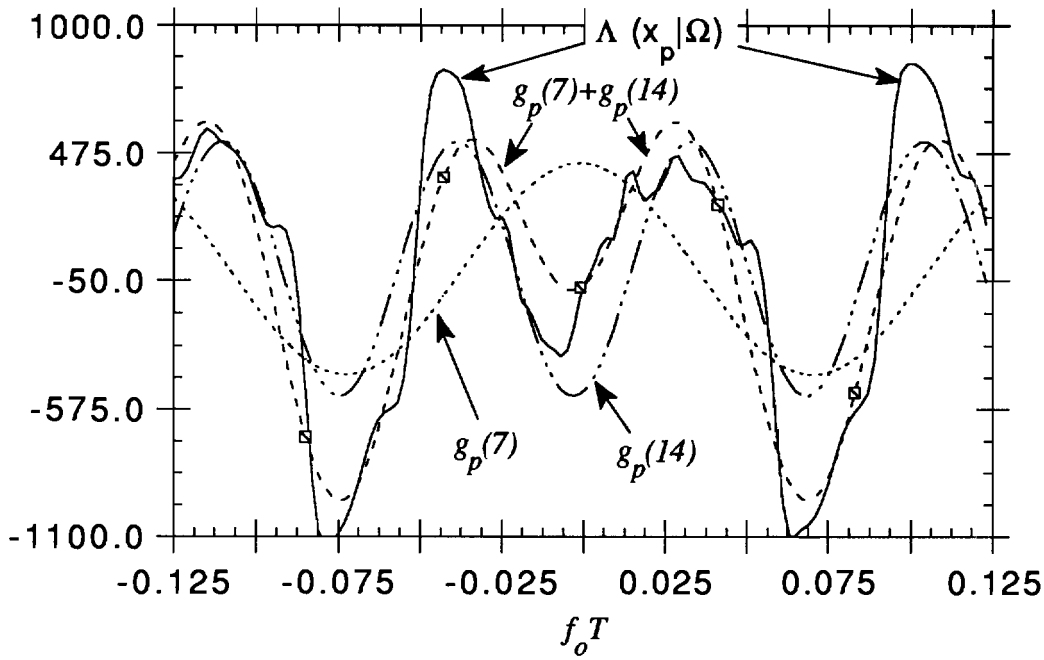

Figure 7.2 A realization of $A(\mathbf{x}_p|\Omega)$ as a function of f_oT and the associated contribution of $g_p(n)$.

Basically there does not exist the best performed Ψ_n in Figure 7.1 if all fading situations are considered. However, Ψ_7 and Ψ_{14} can compensate each other all the time. That is, if one performs badly at certain f_D situation, the other always performs well at that situation. Notice that the number of image solutions is proportional to 1/n. That means although Ψ_{21} and Ψ_{28} seem to perform better than Ψ_7 and Ψ_{14}, the more-than-double computation complexity prevents the usage of Ψ_{21} and Ψ_{28}. Also from Figure 7.2, the contribution of $g_p(7)$ and $g_p(14)$ accounts for the dominant part of $A(\mathbf{x}_p|\Omega)$. Therefore only the first two harmonics are recommended to use. Consequently, a linear estimator like (5.23) given as

$$\hat{\Omega} = \frac{\upsilon_7\Psi_7 + 4\upsilon_{14}\Psi_{14}}{\upsilon_7 + 4\upsilon_{14}} \tag{7.9}$$

is used to roughly estimate Ω. With the outputs of this rough estimator being as the smart starting points, the refinement in Sections 5.5 and 5.6 can thus be applied.

Figure 7.3 shows the performance of frequency offset estimation on a typical TDMA burst. Again, the SSNS stands for the smart start Newton search and the SSLUS represents the smart start local uniform search respectively. Four different SSLUS methods as described in Table 7.1 are employed to see the effect of the search parameters including the local search range and the search resolution. Figure 7.3 shows that the larger search range produces better estimate in fast fading situation ($f_DT = 0.05$) while the finer search grid yields more accurate estimate in very slow fading case. However, the performance differences in fast fading case are more evident than that in slow fading case and hence SSLUS-3 or SSLUS-4 is recommended. SSNS performs well in slow fading cases ($f_DT < 0.015$) but reacts poorly in faster fading cases especially when $f_DT = 0.05$. This is because in faster fading cases, the log-likelihood function (7.2) as a function of Ω is more likely to be jagged as shown in Figure 7.2 and makes the Newton method more possibly lock to the local maximum points instead of the global maximum point.

Table 7.1 Search parameters used by 4 different smart start local uniform search methods.

method used	search range	search resolution
SSLUS-1	0.005	0.002
SSLUS-2	0.01	0.003
SSLUS-3	0.015	0.004
SSLUS-4	0.02	0.005

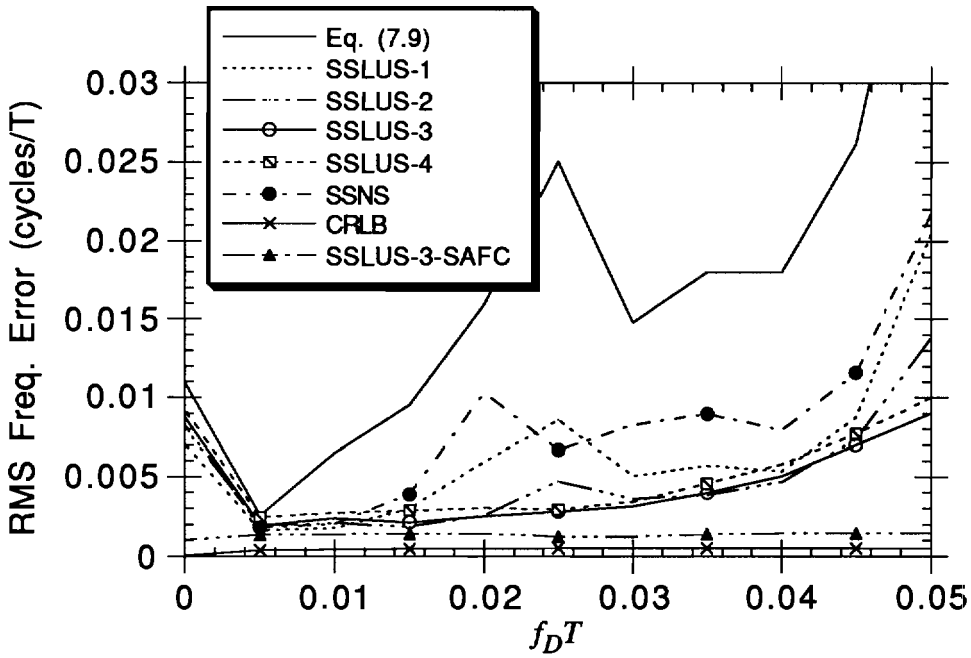

Figure 7.3 Performance of frequency offset estimation for the burst with L=1, S_1=5, S_2=6, P_{ins}=7, N=26, $\overline{E}_{eff}/N_0$ = 20dB, and 100K iterations.

Another feature of Figure 7.3 is that the estimation error by SSLUS-3 or SSLUS-4 first goes down, remain in a flat level, and then goes up in the fast fading case (f_DT > 0.045). This means a little Doppler spread is helpful compared to the static situation (f_D = 0) but a large Doppler spread will do more harm than good. The explanation of this phenomenon is that the motion of the receiver can help the receiver go out of the deep fade zone and suffer less loss than that of static situation (f_D=0) but fast motion of the receiver makes the received sample signal less correlated and hence makes the frequency offset estimator catch the alias frequency more often. Figure 7.4 demonstrates the probability of alias frequency capture in various fading situations. The higher chances in the two ends (of the curve denoted L=1, N=26) match the arguments just mentioned. If the error incurred by alias frequency capture is suppressed from the SSLUS-3, the curve denoted as SSLUS-3-SAFC in Figure 7.3 gives what a normal error should behave. Note

that besides the two causes mentioned above, coarse resolution in the refinement might also result in the alias frequency capture.

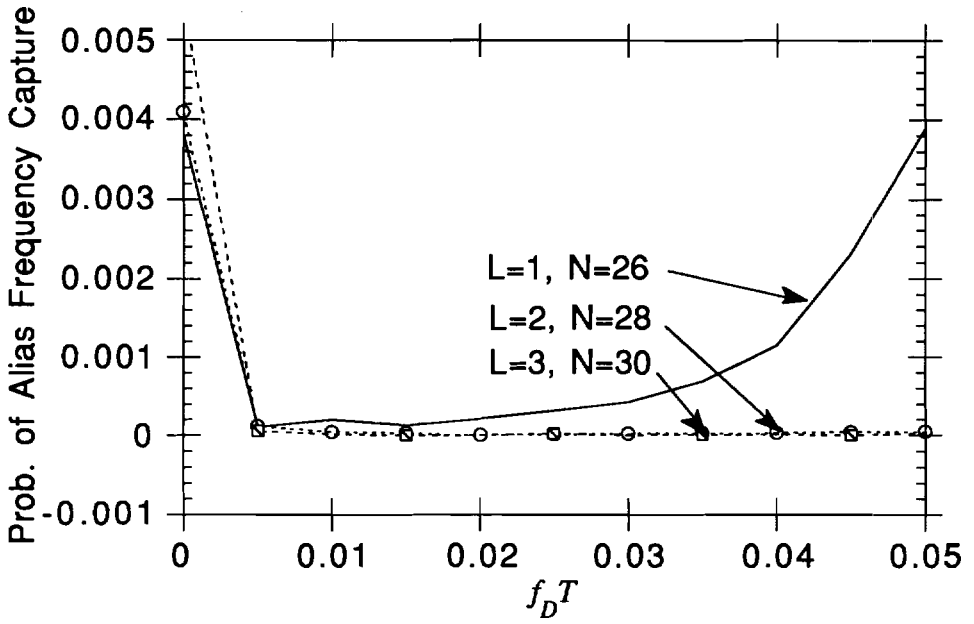

Figure 7.4 Probability of alias frequency capture for TDMA bursts with S_1=5, S_2=6, P_{ins}=7, $\overline{E}_{eff}/N_0$ = 20dB, and 100K iterations.

In later sections, the performance degradation in SNR per bit to maintain certain level of BEP as a function of the RMS frequency error will be investigated. We will see in Figure 7.10 that the amount in RMS frequency error as large as 0.01 will cause significant degradation (more than 5 dB) in the case of f_DT=0.05. This means further reduction in the RMS frequency error in the fast fading case as f_DT=0.05 is desired. Since a large portion of the degradation in RMS frequency error (e.g., deviation from the curve SSLUS-3-SAFC to the curve SSLUS-3 in Figure 7.3) comes from the alias frequency capture effect, to attain more improvement requires elimininating such an effect. Two possible methods can be used to achieve this goal. One is to increase the number of pilot symbols, N_s to let the correlations behave more close to the expected statistics. However, this will make the total burst length longer if the burst structure

remains unchanged. In many applications, this approach turns out to be not ;acceptable. The other way is to change the structure of the burst and specifically give more pilot symbols as the preamble and postamble. Refer to Figure 4.3, this means to use larger values of L instead of L=1 in the case for Figure 7.3.

The reason to assign more pilot symbols in the preamble/postamble instead of in the middle part of the burst (see Figure 4.3 for reference) is two folds. First, as we saw in Figure 4.5(b), larger values of L will have better performance to minimize the positional variation in BEP. Second, the preamble and postamble provide information about lower-step correlations of pilot symbols (e.g., $g_p(1)$ and $g_p(2)$) and will reduce the likelihood of alias frequency capture.

Two alternate frame structures with more pilot symbols in the preamble and postamble are considered for this approach. One is with L=2, N = 28, S_1=5, S_2=6, P_{ins}=7, and the other is with L=3, N = 30, S_1=5, S_2=6, P_{ins}=7. Figure 7.4 tells the probability of alias frequency capture is greatly reduced at f_DT = 0.05 if more preamble and postamble are used. Figure 7.5 shows the estimation performance of the three frame structures considered. Note that the CRLB and the SSLUS-3-SAFC curves of the 3 structures are almost indistinguishable and only those of L=1, N=26 are shown in Figure 7.5. For a clear illustration, the rest of Figure 7.5 only exhibits the curves by SSLUS-3. The reduction in RMS frequency error shows the advantage of using the preamble and postamble for the TDMA aaplication if a fast fading is encountered. Obviously using L=2 works well enough to remove the effect of alias frequency capture in any moving situation (f_DT >0).

The penalty for using the larger number of pilots in the preamble/postamble is the reduced throughput efficiency η, from 144/170=84.7% (for L=1, N=26) to 144/172=83.72% (for L=2, N=28) or 144/174=82.76% (for L=3, N=30) information symbols per T. Compared to the improvement in SNR/bit (see later discussion in Section 7.6), the loss in the throughput efficiency is worth in the tradeoff.

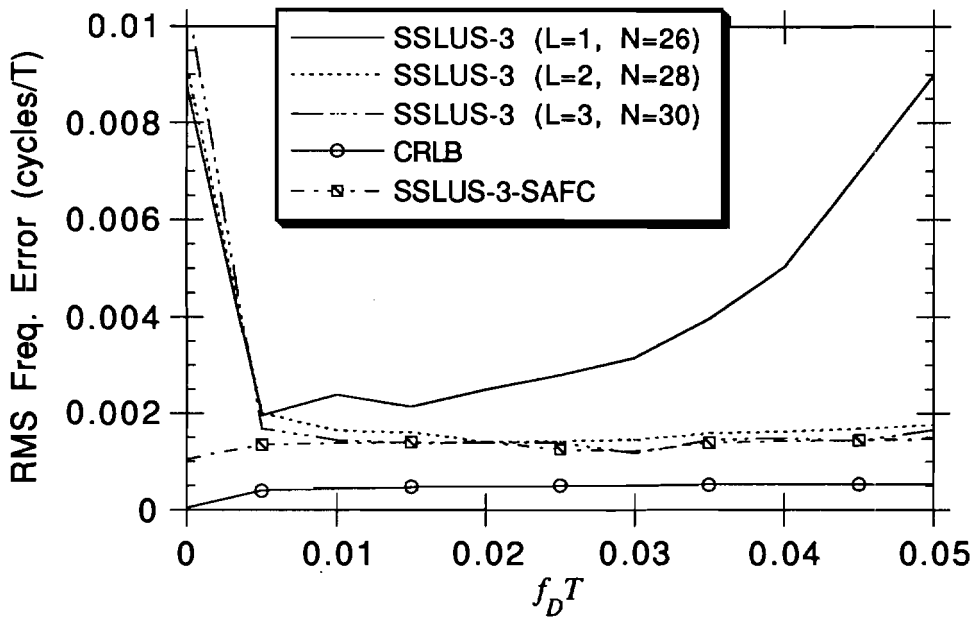

Figure 7.5 Performance of using preamble/postamble in TDMA burst with S_1=5, S_2=6, P_{ins}=7, $\overline{E}_{eff}/N_0$ = 20dB, and 100K iterations.

7.3 For Burst Mode SFH/CDMA

Similar development as in Section 7.2 can be applied to the case of SFH/CDMA. The only difference is that the number of pilot symbols N for a SFH/CDMA hop is smaller. We thus can expect that the performance will be worse than that in TDMA cases and more pilot symbols will be required to be allotted to the preamble/ postamble (i.e., larger L) to reduce the alias frequency capture effect. The recommended structure in Chapter 4 where L=1, S_1=5, S_2=6, P_{ins}=7, and N=11 is first considered here. Figure 7.6 demonstrates the performance of (7.9) and its refinements. The SSLUS and SSNS are the same as described in Section 7.2. The estimation error for the best-performed SSLUS-4 is too huge to accept at f_DT = 0.05. Again, the large portion of error comes from the alias frequency capture. Figure 7.7 shows the probability of alias frequency capture for the example considered (L=1, N=11) at f_DT = 0.05 is as high as 3%. This is because the

number of pilot symbols is not sufficient and makes the alias frequency capture happen more possibly especially in fast fading cases.

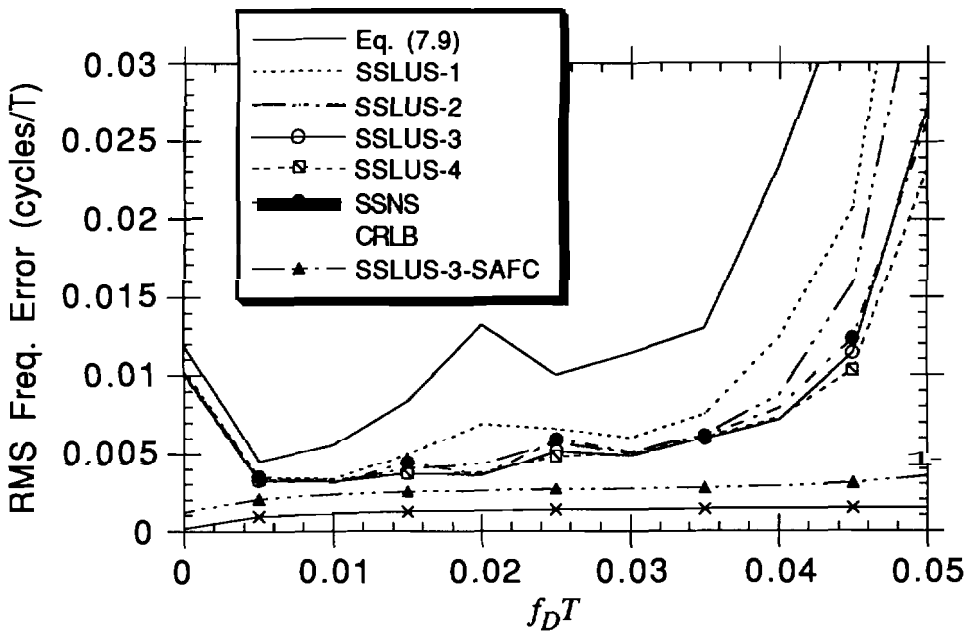

Figure 7.6 Performance of frequency offset estimation for the burst with L=1, S_1=5, S_2=6, P_{ins}=7, N=11, $\overline{E}_{eff}/N_0$ = 20dB, and 100K iterations.

Again, to eliminate the alias frequency capture effect requires more pilot symbols be allotted to the preamble and postamble. Examples considered for SFH/CDMA application in this section ranges from L=2, N=13 to L=5, N=19 where other parameters keep the same, i.e., S_1=5, S_2=6, P_{ins}=7. Figure 7.7 tells how the probability of alias frequency capture is reduced by using larger L. Figure 7.8 shows the estimation performance of these frame structures considered. Again, the CRLB and the SSLUS-4-SAFC curves of the 5 structures are almost indistinguishableand only those of L=1, N=11 are shown. The improvement in performance shows the necessity of the preamble and postamble for SFH/CDMA. For this example, the structure with L=4, N=17 is a recommended choice in the tradeoff between the performance and the throughput efficiency.

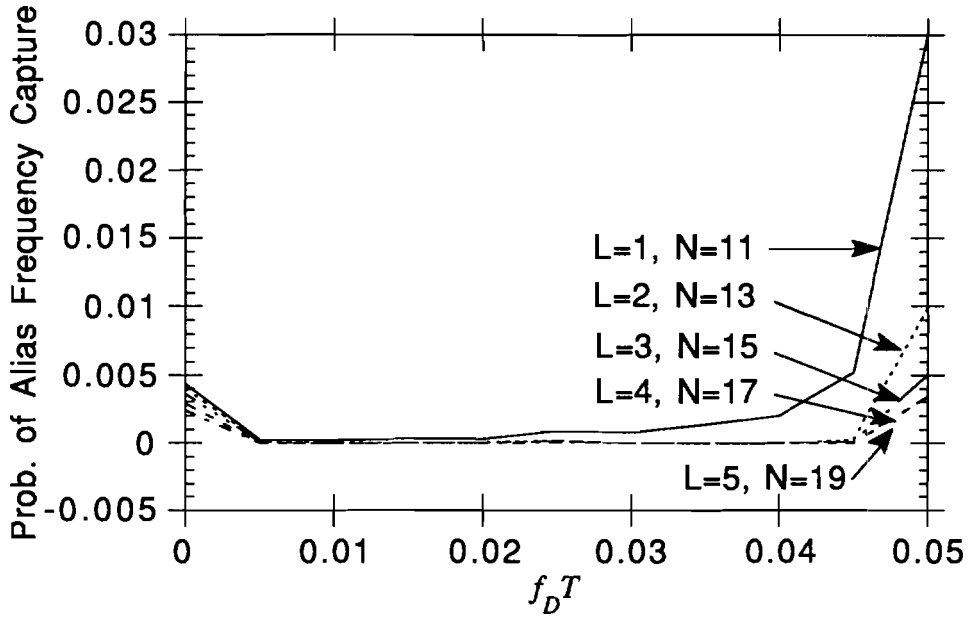

Figure 7.7 Probability of alias frequency capture for the SFH/CDMA bursts with S_1=5, S_2=6, P_{ins}=7, $\overline{E}_{eff}/N_0$ = 20dB, and 100K iterations.

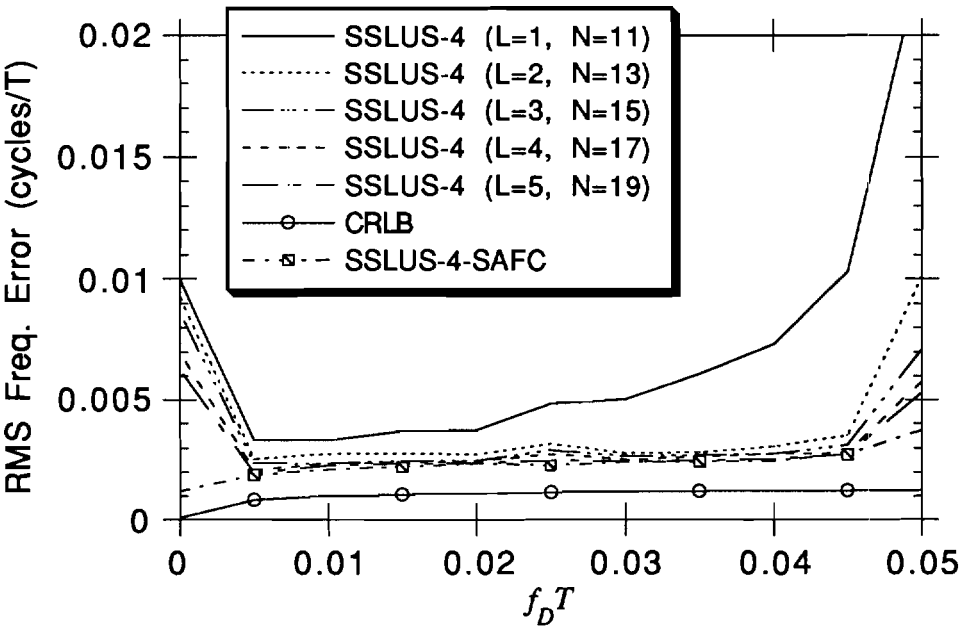

Figure 7.8 Performance of SSLUS-4 for the SFH/CDMA burst with S_1=5, S_2=6, P_{ins}=7, $\overline{E}_{eff}/N_0$ = 20dB, and 100K iterations.

The associated cost of using the preamble and postamble in shorter bursts as SFH/CDMA is more obvious. The decreased throughput efficiencies η, are from 54/65=83.07% (for L=1, N=11) to 54/67=80.6% (for L=2, N=13), 54/69=78.26% (for L=3, N=15), 54/71=76.06% (for L=4 N=17), 54/73=73.97% (for L=5, N=19) information symbols per T.

7.4 BEP with/without Frequency Offset Compensation

In this section, PSAM demodulation with and without frequency offset compensation is modeled by specifying two prototypes of the frequency uncertainty through $p_{f_o}(f_o)$. Recall in Section 3.2, the frequency offset affect the BEP via the Q function as defined in (3.16). The term $E\left[e^{jm\Omega}\right]$ in (2.11) as a component of the autocorrelation of pilot symbols exactly elucidates the effect of frequency uncertainty.

The first model for frequency uncertainty is that $f_oT=\Omega/2\pi$ is uniformly distributed over [-U,U] where $U/(f_cT)$ is the stability margin of the local oscillator and f_c is the carrier frequency. This case accounts for the worst situation that frequency offset is not compensated by any synchronization mechanism. Under such an assumption, in (2.11),

$$E\left[e^{jm\Omega}\right]=\frac{\sin(2\pi mU)}{2\pi mU} \tag{7.10}$$

The second model is that f_oT is Gaussian distributed with zero mean and variance σ_f^2. This case describes the situation that the frequency offset is compensated by a frequency estimator whose residual error after compensation is approximately zero mean Gaussian distributed. Under such a circumstance, the frequency dependent term in (2.11) becomes

$$E\left[e^{jm\Omega}\right]=e^{-2\pi^2m^2\sigma_f^2}. \tag{7.11}$$

By (7.10) and (7.11) with the results in Chapter 3, the BEP performance of a given frame structure can be calculated for systems with or without frequency offset compensation.

7.5 Performance without Compensation

Large degradations in the BEP performance of burst mode PSAM are produced for relatively small frequency offsets if no compensation for a frequency offset is attempted. In this section we assume that f_D is known to the receiver. Define SNR per bit degradation from the ideal carrier case ($f_O T$=0) as

$$SNR/bit\ degradation = 10\log_{10}\left(\frac{the\ \gamma_b\ needed\ to\ attain\ BEP =}{the\ \gamma_b\ needed\ to\ attain\ BEP = 10^{-3}\ if\ f_o T = 0}\right). \quad (7.12)$$

Figure 7.9 shows the SNR/bit degradation from the known carrier frequency case for both long burst and medium length burst applications in cases of $f_D T$=0.03 and 0.05 respectively. The BEP performance is evaluated at the center data synnbol of each burst. Figure 7.9 reveals a BEP threshold phenomenon with U. When U exceeds certain amount, an irreducible BEP occurs. Figure 4.8 has illustrated the combined effect of $f_D T$ and $f_O T$ in the frequency spectrum and the alias property in the spectrum explains the cause of this threshold phenomenon.

Significant performance improvement can be achieved by implementing a frequency estimator if the frequency uncertainty is significantly large. Also note that Figure 7.9 shows the SNR/bit degradation in dB is linearly proportional to U before the threshold is reached. Therefore the reduction of frequency offset uncertainty can provide a notable improvement in the link margins.

7.6 Performance with Compensation

This section examines the performance improvement when a frequency offset estimator is used in conjunction with PSAM processing. Again, f_D is assumed known to the receiver. The $f_O T$ here is assumed to be Gaussian distributed with zero mean and variance σ_f^2. This assumption models the case when an unbiased frequency estimator is used and the resultant root mean square (RMS) frequency estimation error is σ_f. Figure 7.10 shows the SNR/bit degradation from ideal carrier frequency recovery in both long

and medium length burst applications. The performance is evaluated at the center data symbol of the burst.

Since the frequency offset estimators introduced are all based on the maximum likelihood principle, the resulting residual frequency error can be viewed as an approximated Gaussian random variable. The associated effect on error performance of the estimators can be obtained by corresponding the RMS frequency error to Figure 7.10. For example, suppose the frequency uncertainty made by the local oscillator is U=0.03. Then Figure 7.9(a) tells the performance degradation is 2 dB in SNR/bit if no frequency offset compensation is attempted and the burst with L=2, S_1=5, S_2=6, P_{ins}=7, N=28, 64-QAM modulation, and f_DT=0.03 is considered. Figure 7.5 tells that the RMS frequency error can be reduced to 0.0018 at f_DT=0.03 if SSLUS-3 is employed and Figure 7.10(a) shows this amount of frequency error only causes 0.3 dB performance degradation in SNR/bit. The net gain is thus 1.7 dB SNR/bit.

In general, Figure 7.10 unveil the allowable range and the associated performance loss of the RMS frequency error. The specification of a frequency offset estimator to be used in conjunction with PSAM can thus be set accordingly. For example, if the frame structure in Figure 7.10(a) with 16QAM is adopted and the maximum f_DT encountered is 0.03, then the standard deviation (σ_f) of the frequency offset estimator is permitted up to 0.012 without an irreducible BEP. If the system specification allows only 1dB SNR/bit loss due to f_oT, then σ_f must be smaller than 0.005. If lower loss (e.g., 0.5dB) is desired, σ_f must be even smaller (<0.0028). There also exist the similar threshold phenomena for the curves in Figure 7.10 as those in Figure 7.9. Basically the equivalent "bandwidth" of the Gaussian distribution is the counterpart of the U factor in the uniform distribution and the combined effect of f_DT and f_oT produce similar characteristics.

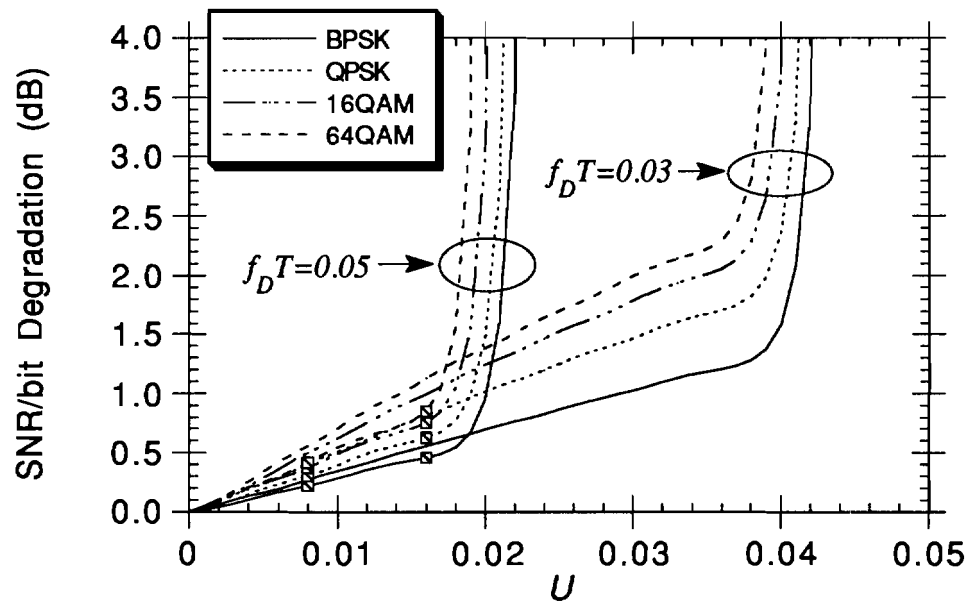

(a) L=2, N=28.

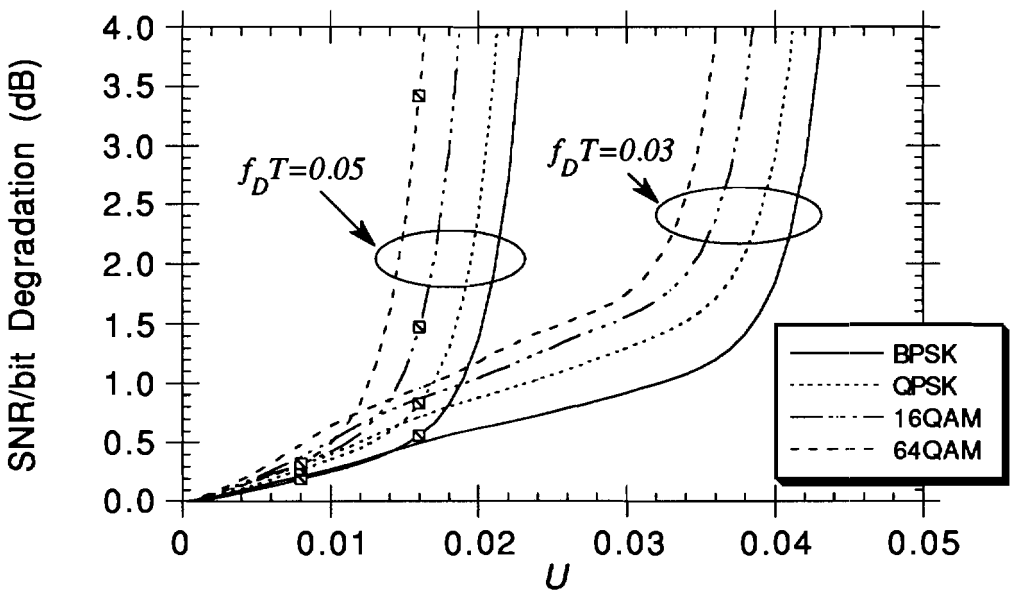

(b) L=4, N=17.

Figure 7.9 SNR degradation versus U. The results are for the center data symbol of the bursts with S_1=5, S_2=6, P_{ins}=7.

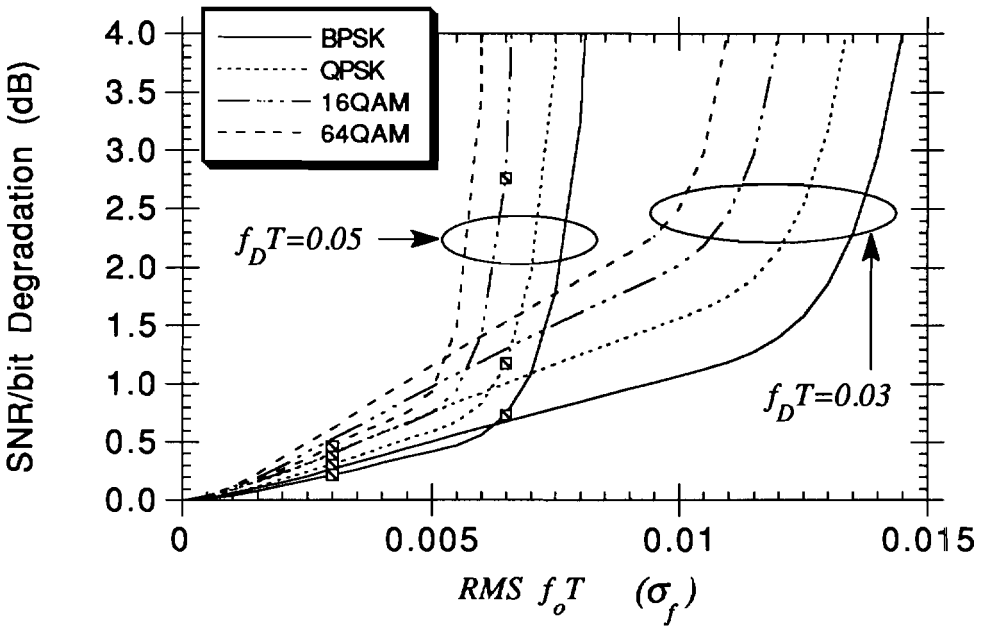

(a) L=2, N=28

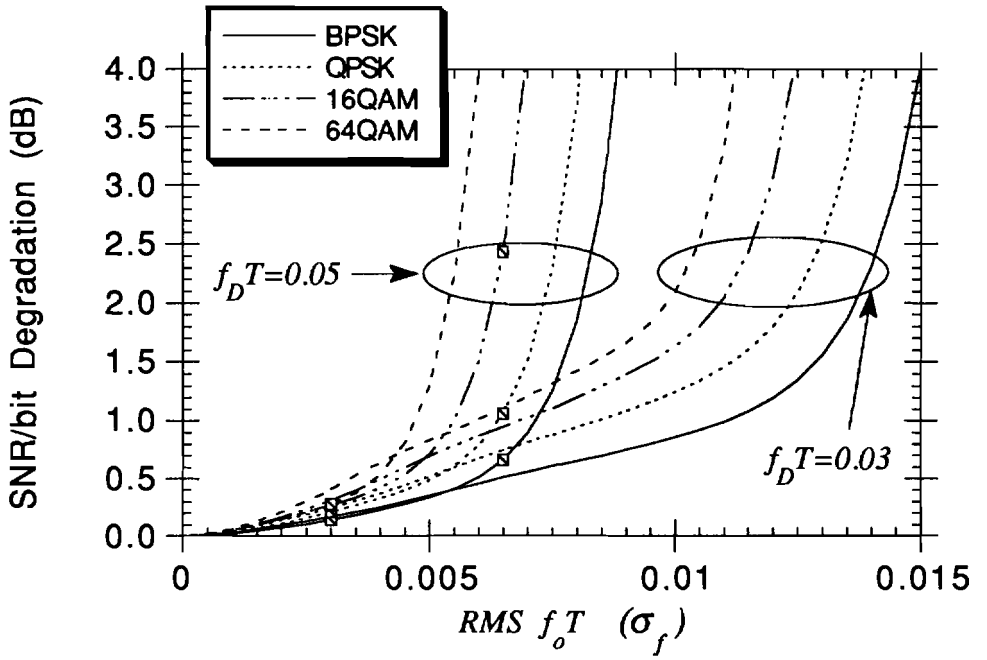

(b) L=4, N=17.

Figure *7.10* **Effect of frequency offset compensation. The results are for the center data symbol of the burst with S_1=5, S_2=6, and P_{ins}=7 where the residual f_oT is assumed Gaussian distributed with zero mean and variance σ_f^2.**

8. CONCLUSION

8.1 Summary of Results

General formulas of BEP as functions of the pilot allocation, Doppler spread, frequency offset and linear modulation scheme are developed in this work. In a burst mode architecture, the performance of the periodic pilot insertion structure prevalent in continuous transmission systems has been found poor in the two edges of a burst. A method to overcome this drawback is to increase the density of pilot symbols in the two ends of a burst. Useful tools to find the better ways to scatter the pilot symbols have been introduced. Trade-off between the performance and the throughput rate has also been considered. For shorter burst applications (like SFH/CDMA) the performance is more sensitive to the positioning of the pilots within burst structure. The effect of unknown Doppler spread has also been studied. The result suggests that some means of Doppler spread estimation can provide a notable (up to 2.5dB) improvement in SNR/bit.

Frequency offset estimation based on the transmitted references in Rayleigh flat fading channels has been well investigated in this work. In continuous operation, the Cramer-Rao performance bound is studied and a near-optimal estimator by smart start local uniform search is introduced. For less complexity implementation, the frequency offset estimator based on the estimated uniform weighting autocorrelation of pilot symbols is investigated. A method of combining the multiple lag correlation terms to produce a better estimate of frequency offset is discovered. The associated implementation is simple and the performance is satisfying even in a very fast fading situation.

For burst mode operation, the associated optimal and near-optimal methods of frequency offset estimation are introduced. Examples for TDMA and SFH/CDMA are also provided. Simulation shows the short burst length of SFH/CDMA necessitates the usage of the preamble and postamble to reduce the chance of alias frequency capture and obtain a better carrier recovery. Basically a frequency offset less than half of the symbol rate can be reduced to less than 0.6% of the symbol rate statistically.

The effect on error performance by frequency offset compensation is also studied. This work reveals frequency estimation can provide a similar performance improvement as in the case of Doppler spread estimation. Since the maximum encountered $f_D T$ is determined by the carrier frequency, the maximum moving speed, and the data symbol rate, it cannot be reduced once the specification is set. To achieve higher throughput rate and maintain a good performance level, some frequency offset estimator must be invoked. Results in Chapters 5-7 provide the implementation choices of the frequency offset estimators. The appropriate specifications of both the frequency offset estimator and the Doppler spread estimator can be settled by the plots shown in this work or by substituting the actual parameters in the associated formulas. Adding such a frequency offset estimation mechanism to the synchronizer can lead to a strong relief in oscillator requirement or equivalently a significant increase in data throughput rate (by allowing larger pilot insertion spacing).

8.2 Future Research

Topics for further efforts on transmitted references can be a long list. Continuing research based on the available results includes the following.

1) A high performance Doppler spread estimator. Section 4.5 has studied the performance degradation of the mismatch of Doppler spread. It suggests that implementing a good Doppler spread estimator can lead to up to 2.5 dB gain in SNR per bit. The first idea for Doppler spread estimation is that the "bandwidth" of the main lobe

in the spectrum of log-likelihood function (as a function of Ω shown in Figure 7.2) is closely related to the Doppler spread. Also note that (5.15) and (6.1) tell that the amplitude of the sample autocorrelation function of pilot symbols is a Bessel function of the Doppler spread. These evidences provide the direction to start. Explicit relation between Doppler spread and the pilot correlation is a breakthrough to explore.

2) Consideration in frequency selective fading channels. For a wide time-dispersive delay spread, a frequency selective fading environment is resulted. Burst design, frequency offset estimation, and the associated performance effect require more sophisticated treatment and analysis. The ISI caused by the frequency offset in this situation is an issue worthy of investigation.

3) PSAM demodulation based on the array receiver. Recent research [30] has succeeded in using an array receiver to resolve multiple arrivals from various angles. Basically each resolved signal is representative of a transmission path and suffers different fading and delay. How to optimally combine these replicas of faded signal to demodulate can be a rewarding investigation.

LIST OF REFERENCES

[1] A. Aghamoharnmadi and H. Meyr, "A New Method for Phase Synchronization and Automatic Gain Control for Linearly Modulated Signals on Frequency Flat Fading Channels," *IEEE* Trans. Commun., vol. COM-38, January 1991, pp. 25-29.

[2] A. Aghamohammadi, H. Meyr, and G. Ascheid, "Adaptive Synchronization and Channel Parameter Estimation Using an Extended Kalman Filter," *IEEE* Trans. Commun., vol. COM-37, November 1989, pp. 1212-1219.

[3] T. Alberty and V. Hespelt, "A New Pattern Jitter Free Frequency Error Detector," *IEEE* Trans. Commun., vol. COM-37, February 1989, pp. 159-163.

[4] S. Bellini, C. Molinari, and G. Tartara, "Digital Frequency Estimation in Burst Mode QPSK Transmission," *IEEE* Trans. Comm., vol. COM-38, July 1990, pp. 959-961.

J.K. Cavers, "An Analysis of Pilot Symbol Assisted Modulation for Rayleigh Faded Channels," *IEEE* Trans. Veh. Technol., vol. VT-40, November 1991, pp. 686-693.

J.K. Cavers, "Performance of Tone Calibration with Frequency Offset and Imperfect Pilot Filter," *IEEE* Trans. Veh. Technol., vol. VT-40, May 1991, pp. 426-434.

[7] J.K. Cavers and P. Ho, "Analysis of the Error Performance of Trellis-Coded Modulation in Rayleigh Fading Channels," *IEEE* Trans. Commun., vol. COM-40, January 1992, pp. 74-83.

[8] J.K. Cavers and J. Varaldi, "Cochannel Interference and Pilot Symbol Assisted Modulation," *IEEE* Trans. Veh. Technol., vol. VT-42, November 1993, pp. 407-413.

[9] J.C.-J. Chuang and N.R. Sollenberger, "Burst Coherent Detection with Combined Symbol Timing, Frequency Offset Estimation, and Diversity Selection," *IEEE* Trans. Commun., vol. COM-39, July 1991, pp. 1157-1164.

[10] F. Classen, H. Meyr, and P. Sehier, "Maximum Likelihood Open Loop Carrier Synchronizer for Digital Radio," 1993 *IEEE* International Conference on Communications, Geneva, Switzerland, pp. 493-497.

[11] S.N. Crozier, D.D. Falconer, and S.A. Mahmoud, "Reduced Complexity Short-Block Data Detection Techniques for Fading Time-Dispersive: Channels," *IEEE* Veh. Tech., VT-41, August 1992, pp. 255-265.

[12] F. Davarian, "Mobile Digital Communication Via Tone Calibration," IEEE Trans. Veh. Tech., vol. VT-36, May 1987, pp. 55-62.

[13] D. Divsalar and M.K. Simon, "Multiple-Symbol Differential Detection of MPSK," IEEE Trans. Commun., vol. COM-38, March 1990, pp. 300-308.

[14] M.P. Fitz, "A Dual-Tone Reference Digital Demodulator for Mobile Digital Communications," IEEE Trans. Veh. Technol., vol. VT-42, May 1993, pp. 156-165.

[15] M.P. Fitz, "Further Results in the Fast Estimation of a Single Frequency," IEEE Trans. Commun., March 1994,

[16] M.P. Fitz and J.P. Seymour, "On the Bit Error Probability of QAM Modulation," International J. Wireless *Inform*. Networks, vol. 1, April 1994,

[17] F.M. Gardner, "Characteristics of Frequency-Tracking Loops," IE'EE Trans. Commun., vol. COM-33, February 1985, pp. 131-139.

[18] R. Haeb and H. Meyr, "A Systematic Approach to Carrier Recovery and Detection of Digitally Phase Modulated Signals on Fading Channels," IEEE Trans. Commun., vol. COM-37, July 1989, pp. 748-754.

[19] P. Ho and D. Fung, "Error Performance of Multiple-Symbol Differential Detection of PSK Signals Transmitted Over Correlated Rayleigh Fading Channels," IEEE Trans. Commun., vol. COM-40, October 1992, pp. 1566-1569.

[20] W.C. Jakes, Microwave Mobile Communications, Wiley, New York, 19'74.

[21] S. Kay, "A Fast and Accurate Single Frequency Estimator," IEEE *Trans. Acoust.*, Speech, Signal Processing, vol. ASSP-37, December 1989, pp. 1987-1990.

[22] W.C.Y. Lee, Mobile Communications Engineering, McGraw-Hill, New York, 1982.

[23] M. Luise and R. Reggiannini, "An Efficient Carrier Frequency Recovery Scheme For GSM Receivers," 1992 IEEE Global Telecommunications Conference, Orlando, FL, pp. 36-40.

[24] W.F. McGee, "Complex Gaussian Noise Moments," IEEE Trans. Info. Theory, vol. IT-17, March 1971, pp. 149-157.

[25] K.S. Miller, Multidimensional Gaussian Distributions, John Wiley & Sons Inc., New York, 1964.

[26] M.L. Moher and J.H. Lodge, "TCMP - A Modulation and Coding Scheme for Rician Fading Channels," IEEE J. Select. Areas Commun., vol. SAC-7.,December 1989, pp. 1347-1355.

[27] F.D. Natali, "AFC Tracking Algorithms," IEEE Trans. on Comm., vol.. COM-32, August 1984, pp. 935-947.

[28] J.G. Proakis, Digital Communications, McGraw -Hill, New York,,1989.

[29] S. Saito and H. Suzuki, "Fast Carrier-Tracking Coherent Detection with Dual-Mode Carrier Recovery Circuit for Digital Land Mobile Radio Transmission," IEEE J. Select. Areas Commun., vol. 7, January 1989, pp. 130-139.

[30] J.J. Shynk and R.P. Gooch, "Cochannel Signal Demodulation Using the CMA Adaptive Beamformer," 1994 Globecom, under review.

[31] S. Stein, "Unified Analysis of Certain Coherent and Noncoherent Binary Communication Systems," IEEE Trans. Info. Theory, vol. IT-10, February 1964, pp. 43-51.

[32] H.L. Van Trees, Detection, Estimation, and Modulation Theory, John Wiley & Sons, New York, 1968.

[33] A.J. Viterbi and A.M. Viterbi, "Nonlinear Estimation of PSK Modulated Carrier Phase with Application to Burst Digital Transmission," IEEE Trans. Info. Theory, vol. IT-32, July 1983, pp. 543-551.

[34] W.J. Weber III, "Performance of Phase-Locked Loops in the Presence of Fading Communications Channels," IEEE Trans. *Commun.*, vol. COM-24, May 1976, pp. 487-499.